

AD-A278 963



Technical Document 2591
December 1993

Performance Criteria for Coherent Interping Reverberation Suppression

Doug Grimmett
NRaD
Xavier Zabai
Alliant Tech Systems

DTIC
ELECTE
MAY 06 1994
S G D

94-13703



Approved for public release; distribution is unlimited.



94 5 05 154

Technical Document 2591
December 1993

Performance Criteria for Coherent Interping Reverberation Suppression

Doug Grimmett
NRaD
Xavier Zabal
Alliant Tech Systems

Accession For	
NTIS CRA&I	<input checked="" type="checkbox"/>
DTIC TAB	<input type="checkbox"/>
Unannounced	<input type="checkbox"/>
Justification	
By	
Distribution /	
Availability Codes	
Dist	Avail and/or Special
A-1	

CONTENTS

INTRODUCTION	1
ACTIVE SONAR SOURCE	2
ACTIVE SONAR SIGNAL PROCESSING	3
DATA COLLECTION	3
COMPLEX DEMODULATION	3
BEAMFORMING	4
MATCHED FILTER	4
REVERBERATION SUPPRESSION	4
NORMALIZATION, THRESHOLDING, AND DETECTION	4
SONAR SYSTEM GEOMETRY	4
REVERBERATION-LIMITED ENVIRONMENT	7
COHERENT REVERBERATION SUPPRESSION	8
ADAPTIVE REVERBERATION-SUPPRESSION ALGORITHMS	11
INTERPING COHERENCE	13
REVERBERATION POWER REDUCTION (CASE 1)	15
REVERBERATION POWER REDUCTION (CASE 2)	17
COHERENCE OF REVERBERATION	18
TARGET ECHO LOSSES	21
GAIN AGAINST REVERBERATION	31
VALIDATION WITH DATA	32
SUMMARY	40
REFERENCES	40
FIGURES	
1. Acoustic ping transmitting sequence.	2
2. Typical active sonar signal processing path.	3
3. Sonar system geometry (bistatic).	5
4. Equitime ellipses and blanking region.	6
5. Typical matched filter output, noise-limited.	7

6. Typical matched filter output, reverberation-limited.	9
7. Reverberation processing and interping coherence.	10
8. Adaptive suppression using LMS or RLS (Case 1).	11
9. Adaptive suppression using SVD (Case 2).	13
10. Theoretical RPR_1 vs. interping coherence.	17
11. Theoretical RPR_2 vs. interping coherence.	18
12. Maximum coherence obtainable vs. RNNR.	20
13. Theoretical RPR_1 vs. input RNNR ($N = 2$).	21
14. Theoretical RPR_2 vs. input RNNR ($N = 5$).	21
15. Modulated sinc function ($f_c/B = 3.33$).	23
16. Echo loss vs. echo time shift ($f_c/B = 1.67$).	24
17. Echo loss vs. echo time shift ($f_c/B = 3.33$).	24
18. Echo loss vs. echo time shift ($f_c/B = 6.67$).	25
19. Echo loss vs. echo time shift ($f_c/B = 13.33$).	25
20. Echo loss, theory vs. simulation (nonadaptive).	26
21. Echo loss, theory vs. simulation (RLS).	27
22. Echo loss envelopes ($B = 10$).	28
23. Echo loss envelopes ($B = 20$).	28
24. Echo loss envelopes ($B = 30$).	29
25. Echo loss envelopes ($B = 40$).	29
26. Echo loss envelopes for varying repetition rates.	30
27. Echo loss envelopes for varying target Dopplers.	30
28. Received ping sequence of reverberation data.	33
29. Interping coherence measurement, ping 1 and ping 2.	34
30. Interping coherence functions.	35
31. Theoretical reverberation power reduction.	35
32. Output of reverberation-suppression processing.	37
33. Reverberation power reduction achieved.	37
34. RPR_1 achieved vs. theory ($N = 2$).	38
35. RPR_2 achieved vs. theory ($N = 5$).	38
36. Estimation of coherence of reverberation.	39

INTRODUCTION

Active sonar surveillance systems typically experience diminished detection performance in reverberation-limited environments. In some underwater environments, the transmission of an active sonar pulse leads to acoustic reflections from the ocean bottom, from the sea surface, and from within the ocean volume. These reflections can have significant power levels at the receiver and may present a background level that is higher than the level of the local ambient noise. This is known as a reverberation-limited environment, because it is the reverberation and not the ambient noise that limits detection performance^[1]. In such an environment, target echoes may not be strong enough to be detectable above the reverberation level, being masked by it. The amount of reverberation experienced is variable, depending largely on the oceanographic conditions, acoustic propagation, and surrounding bathymetry. In addition, reverberation levels are dependent on source levels and the transmitted pulse characteristics, such as center frequency, bandwidth, and duration. There are a variety of approaches and methodologies that reduce the adverse effect of reverberation, enabling the detection of targets of interest.

In an active sonar system, the effect of reverberation can be reduced by either the spatial or temporal processing of the received signals. In spatial processing, adaptive beamforming can reduce signal leakage through the beams' sidelobes that are due to strong reverberation features. This is done by steering nulls in the directions of the interferers. Reverberation reduction by temporal processing is based on the ability to discriminate a target signature from the low Doppler reverberation field. This may be done with the use of Doppler-sensitive waveforms, adaptive Doppler filtering, or coherent multiping processing.

The temporal multiping processing methods used to reduce reverberation are referred to as ping-to-ping or coherent interping reverberation-suppression techniques. These methods are based on the assumption that the characteristics of the contaminating reverberation are similar from one received transmission to the next. If this assumption holds, then by using other received transmissions as reference signals, it is possible to subtract out the common reverberation they share, from the received input signal. The reference signals are usually taken from prior or subsequently received pings. The subtraction is actually implemented with an adaptive digital filter in order to optimize the reduction of the reverberation.

The adaptive suppression algorithms can be implemented and applied to datasets, and the resulting performance gains can be measured. Many of the adaptive algorithms require input parameters, and their performance is sensitive to them. In addition, the performance of these techniques depends on the characteristics of the acoustic dataset itself. Therefore, it is important to be able to determine the limits of performance by using these techniques on a particular dataset. This can be done in large part with the interping coherence measurement.

The interping coherence measurement can be made on the dataset, and from it, theoretical performance gains can be determined. The ability to predict the amount of gain obtainable against reverberation is valuable, because it enables the assessment of the effectiveness of these techniques on the dataset. Then, if the data are processed using one of the suppression algorithms, the parameters may be adjusted until the theoretical gains are achieved.

While it is possible to suppress reverberation using these techniques, it is also possible that the target echo undergoes suppression as well. For these techniques to be effective, it is essential that the target echo is preserved, while only the reverberation is suppressed. In order for the target echo to be preserved, it must decorrelate from ping to ping. This implies some target motion. Therefore, target motion relative to the source and receiver affects the suppression techniques' ability to preserve target echoes.

This report addresses the performance criteria of ping-to-ping reverberation-suppression techniques. First, typical sonar signal processing methods and the sonar system geometry are reviewed. Then, the interping coherence measurement and the effects of target motion are addressed. Finally, interping coherence measurements and suppression results are shown for some reverberation data collected at sea, as validation of the algorithms' performance.

ACTIVE SONAR SOURCE

Consider an acoustic source that transmits a sequence of N identical signals, as shown in figure 1. Assume that each individual pulse, $p(t)$, is time varying, of finite duration, T_p , and of bandwidth B . Let the ping repetition interval be T_{pri} , such that the total source transmission sequence is given by

$$p_{seq}(t) = \sum_{k=1}^N p[t - (k - 1)T_{pri}] = \sum_{k=1}^N p_k(t) \quad (1)$$

where $T_{pri} > T_p$ and $p_k(t)$ is the k^{th} ping of the sequence. The transmitted pings are assumed to be frequency modulated or broadband waveforms, and insensitive to Doppler shifts. These types of signals are used because of their excellent range-resolution properties. Generally, the source array has vertical aperture to provide directionality, and it transmits in all azimuthal directions. The acoustic transmissions are then propagated through the acoustic channel. The transmissions may experience amplitude fluctuations, phase shifts, boundary interactions, and propagation over multiple paths by the time they arrive at the receive array.

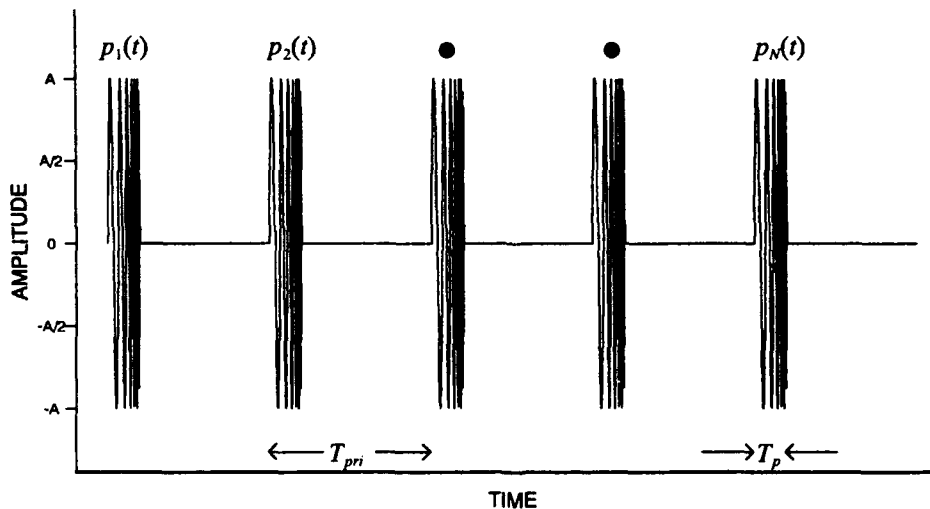


Figure 1. Acoustic ping transmitting sequence.

ACTIVE SONAR SIGNAL PROCESSING

Active sonar systems typically perform signal processing functions on the received data similar to those shown in figure 2. Each block in the processing chain is summarized below.

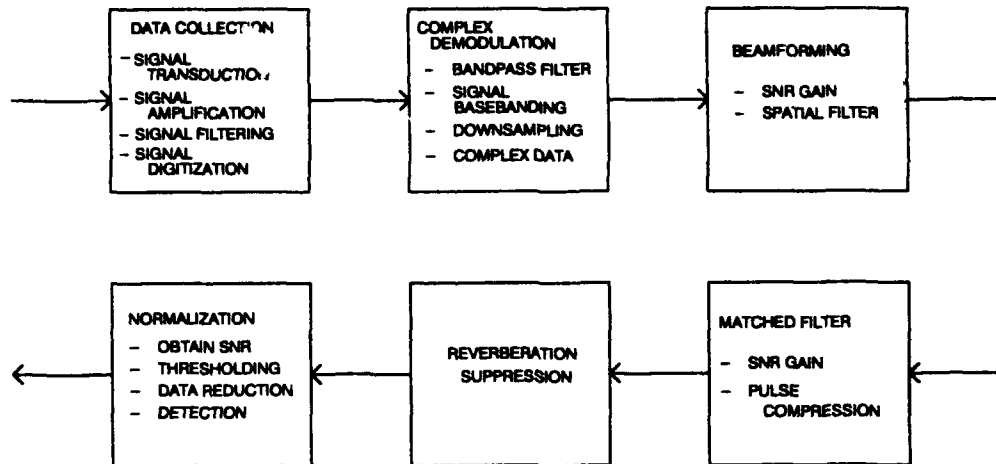


Figure 2. Typical active sonar signal processing path.

DATA COLLECTION

Sonar receive arrays are composed of multiple acoustic sensors, put together in a variety of configurations, spacings, and apertures. Each hydrophone transducer senses the pressure incident upon it and converts the acoustic signal into a voltage. The voltage signals are then passed through the receiver electronics, where they may be conditioned, amplified, and filtered. Following this, the signals are digitized with the use of an analog-to-digital converter. With the data in digital form, the remaining signal processing functions can be efficiently implemented using digital hardware and software.

COMPLEX DEMODULATION

In active sonar, except for small Doppler shifts, returning echoes occupy roughly the same frequency band as the transmitted ping. Since everything of interest is within this band, it is desirable to filter around it. Bandpass filtering over the frequency extent of the waveform effectively eliminates the contamination of out-of-band noise, thereby increasing the signal-to-noise ratio. Once the signal frequency band is passed, it is possible to demodulate the data, from the ping's center frequency down to zero. The resulting basebanded data are complex-valued, which is a convenient form for the signal processing functions that follow. In addition, demodulation makes it possible to reduce the input data sample rate down to the new Nyquist frequency, which corresponds to the bandwidth passed by the filter. This filtering is similarly done on all the available hydrophone element data.

BEAMFORMING

With an array of sensors it is advantageous to sum all the available hydrophone signals, with appropriate delays, thereby enhancing the signal-to-noise ratio. This beamforming process also provides the spatial discrimination of a signal's arrival, which is unobtainable with a single omnidirectional hydrophone. Multiple beams can be formed simultaneously, and steered to look in specified directions, to provide the desired spatial coverage.

MATCHED FILTER

Because the transmitted pulse is known, active sonar processors typically make use of the matched filter. A matched filter correlates the received data stream with a replica of the transmitted pulse. The matched filter provides a signal-to-noise ratio gain when the replica matches up with similar signals in the received data stream. In addition, when frequency-modulated broadband pulses are used, the matched filter compresses any echoes into sharp peaks. This pulse-compression property is desirable, because it allows for the resolution of echoes at time differences equal to the reciprocal of the bandwidth. In addition, any effective Doppler shift in the echo will translate directly into a time shift of the correlation peak. The matched filtering is performed on each of the output beams. At the output of the matched filter, target echoes may be searched for on the square of the magnitude of the complex data, which is the signal's power.

REVERBERATION SUPPRESSION

At this stage of the processing, although the signal-to-noise ratio has been significantly increased, target echoes may or may not be detectable above the noise or reverberation background level. If the desired target echo is above the ambient noise background, but obscured by a distributed reverberation background, then further processing may improve detection performance. In such an event, interping reverberation subtraction techniques may be employed to an advantage, by suppressing the obscuring reverberation. Multiple pings are collected and then input into an adaptive interference-cancellation filter.

NORMALIZATION, THRESHOLDING, AND DETECTION

The processed data are normalized as a part of detection processing. The normalizer outputs a sequence from which the signal power to local background (noise or reverberation) power ratio can be obtained. This ratio is a measure of the echo's detectability. In the noise-limited case, these values can be thought of as the signal-to-noise ratio. A threshold is then applied to the normalized data, with only the data that are above the threshold passed on to the detector. The detector may either be an automated computer algorithm providing alerts or a human operator using graphical displays. Detection processing is performed on each of the matched filter beam outputs.

SONAR SYSTEM GEOMETRY

Consider the bistatic sonar geometry as described by Cox^[2], and as shown in figure 3. A bistatic geometry is the most general one, in which the active source and receiver are in different

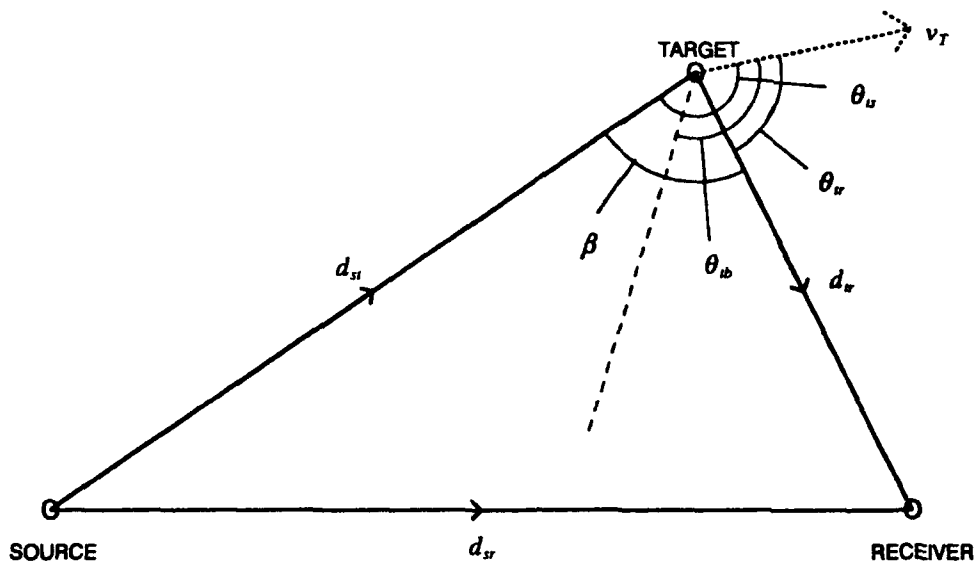


Figure 3. Sonar system geometry (bistatic).

physical locations. The transmitted signals travel from the source to the receiver along the direct path d_{sr} . The reception of this signal in the received data stream is called the “direct blast,” and it typically has very high power, since the acoustic energy is transmitted with very high power and undergoes only one-way attenuation. Assume that the transmitted pulse also travels to a target of interest along the path d_{st} , is reflected from the target, and travels along the path d_{tr} to the receiver. The total target range in this configuration is d_{tot} , which is equal to the sum of d_{st} and d_{tr} . The propagation path for the target echo is longer than the direct path, by an additional distance d_e , given as

$$d_e = d_{tot} - d_{sr} = d_{st} + d_{tr} - d_{sr} \quad (2)$$

These ranges can also be described equivalently, in terms of their acoustic travel times, as

$$t_e = t_{st} + t_{tr} - t_{sr} \quad (3)$$

where $t = \frac{d}{c}$ and c is the velocity of sound propagation in the ocean. The time t_e is the time after the arrival of the direct blast that a target echo arrives at the receiver. The source and the receiver positions form the foci of “equitime” ellipses, which are loci of points for which the bistatic travel times are equal. The size of the ellipse corresponds directly to the echo arrival time, t_e . The equitime ellipse for a source–receiver pair is shown in figure 4. In order for the echo to be cleanly received without being masked by the direct blast energy requires that $T_p < t_e$. Echoes from scatterers located inside the equitime ellipse that corresponds to T_p are drowned out by the enormous energy of the direct blast. This area is called the direct blast blanking region.

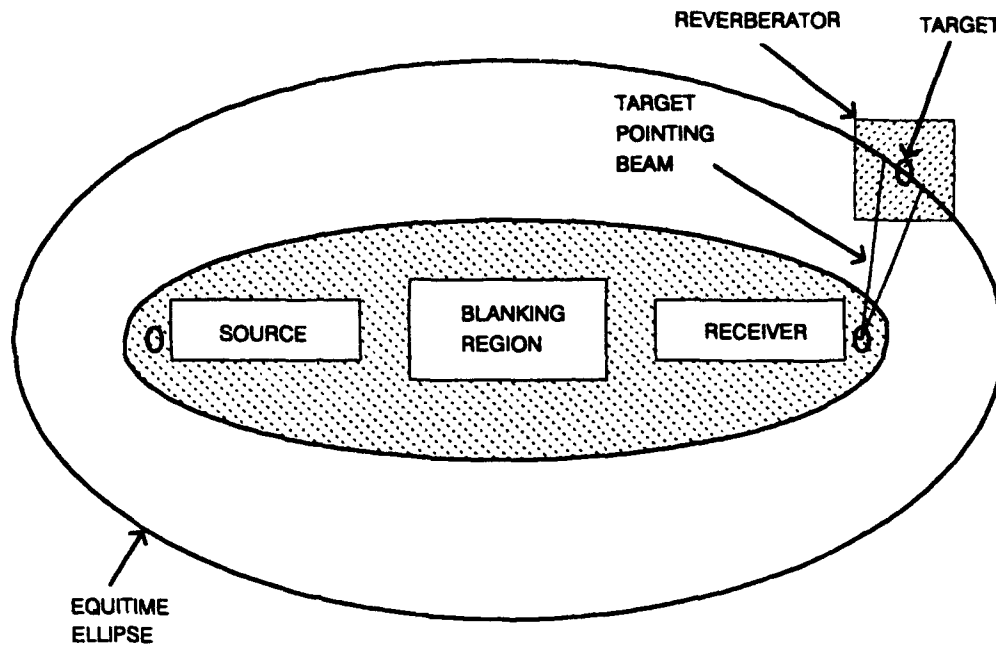


Figure 4. Equitime ellipses and blanking region.

Typically, the bistatic receiver is a horizontal line array of hydrophones, either fixed on the bottom or towed by a moving platform. It typically has a beamforming capability to spatially filter the received data. Beamforming enhances the ability to determine the arrival angle of signals and yields a gain in signal-to-noise ratio. Figure 4 also shows one such beam, pointing in the direction of a target situated in a highly reverberant area populated by a variety of scatterers. In general, for a linear array, there is an ambiguity to the beam steering directions, and the interfering reverberation could be coming in from the front or the back beam direction. In addition, strong reverberation from other directions may leak through the beam's sidelobes, degrading detection performance.

The beam directions and time delays t_e , directly map to azimuthal directions and equitime ellipses, respectively. From the processed data and this mapping, an estimate of the approximate physical location of the echo-producing target can be made. Figure 5 depicts the magnitude of a typical matched filter power output for a target-pointing beam, for a noise-limited case. Note the reception of the direct blast, and at time t_e later, the reception of the target echo.

The sonar geometry has been described for the bistatic configuration. This case is emphasized here, since it is the most general case for a sonar system. The more familiar configuration is monostatic, where the source and the receiver are colocated. The monostatic geometry is just a special case of the bistatic configuration. This occurs when $d_{sr} = 0$, and $d_{st} = d_{tr} = d_t$. Therefore, for the monostatic case, $d_e = 2d_t$. Also, the equitime ellipses lose their eccentricity and become circles.

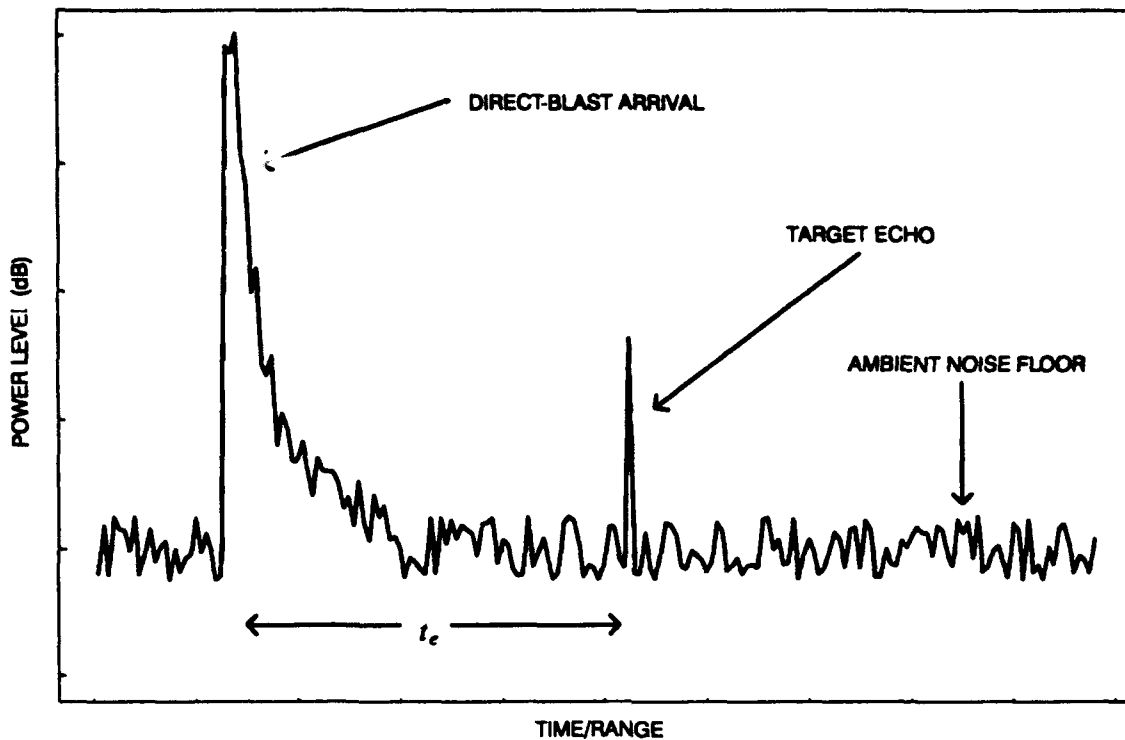


Figure 5. Typical matched filter output, noise-limited.

REVERBERATION-LIMITED ENVIRONMENT

To ensure that received reverberation is similar from ping to ping, only the case where both the source and the receiver positions remain stationary is considered. This kind of bistatic sonar system has a "fixed-fixed" configuration. The fixed-fixed configuration increases the likelihood of having stationary and coherent reverberation in the received data stream from one transmission to another. The receive array receives the direct-blast arrival from the transmitted pulse $p_k(t)$, as well as any scattered reflections from the bottom, from the surface, and from within the ocean volume. In this fixed-fixed configuration, the reverberation echoes associated with each transmission have the best chance of being coherent from ping to ping. Coherence between the reverberation from one ping to the next is a prerequisite for the subtraction algorithms to be effective, and will be demonstrated later in this report.

The received signal x_k , from the k^{th} transmitted pulse p_k , can be characterized as the sum of all the individual reflections from each scatterer, plus the local ambient noise background. Each reverberation feature will have its own scattering strength and will yield a distributed collection of echoes in the received data stream at the appropriate times and in the appropriate beams. Assuming a stationary reverberation field with identical (perfectly coherent) reverberation from ping to ping, each received signal x_k can be given as

$$x_k(t) = r_c(t) + n_k(t) \quad (4)$$

where r_c is the same coherent reverberation component and n_k is the differing local noise signal for each ping.

Now, consider the received reverberation power caused by scattering from the ocean bottom. Pronounced bathymetric features, continental shelves, and the ocean bottom in shallow water tend to be very good scatterers of sound, resulting in an overall increase in the received signal power above that of the ambient background noise power. It is this type of reverberation to which interping reverberation-suppression techniques are best suited, because the properties and statistics of the reverberation are most likely to be the same from transmission to transmission.

The increases in received signal power caused by bottom reverberation occur in the time series data in the same manner as explained previously for target echoes. The time cell of the received reverberation corresponds to an equitime ellipse. The azimuthal direction of the scattered energy may be determined by the formation of multiple beams. A depiction of a single beam's matched filter power output with reverberation features might appear as in figure 6, where the increases in signal power are due to bathymetric features. Notice that when the reverberation power rises above the ambient noise power, the sonar system is reverberation-limited in those regions. In this situation target echoes may be masked and therefore remain undetectable. With these conditions, the suppression techniques may provide detection performance gains by reducing the amount of obscuring reverberation.

COHERENT REVERBERATION SUPPRESSION

Consider a target that is moving with velocity v_T within an area of high bottom reverberation and obscured by it in the matched filter output, as shown in figure 6. In the absence of reverberation, the target echo is detected easily, since it is well above the ambient noise background. Here, however, the reverberation power obscures it. Assume that a ping sequence $p_{seq}(t)$ is transmitted with the same waveform type and with ping repetition interval T_{pri} . The repetition interval is typically chosen so that the reverberation has diminished significantly, to levels below that of the ambient noise background, before the next ping is received. This eliminates undesirable reverberation buildup from one ping to the next. In addition, there may be other factors driving this choice, such as source duty cycle limitations. The acoustic energy propagates to the target and other scatterers, reflects from them, and propagates to the receiver. Figures 7a and 7b depict two consecutively received signals at the output of a matched filter. These pings have been extracted from the received data stream and time-aligned by T_{pri} so that the arrival of their direct blasts line up. Comparing the two pings, it is seen that the reverberation power appears to be similar from ping-to-ping. The reverberation processing is essentially an adaptive subtraction of one ping from another. If the reverberation background is coherent, then the suppression techniques may be effectively applied. Because of the target's motion, its echoes shift in arrival time relative to one another from one ping to the next. With sufficient time shift between the echoes, the input target echo can be passed through the reverberation processing unsuppressed. An example output of the suppression process is depicted in figure 7c. Notice that with the reduction in reverberation, the target has become detectable.

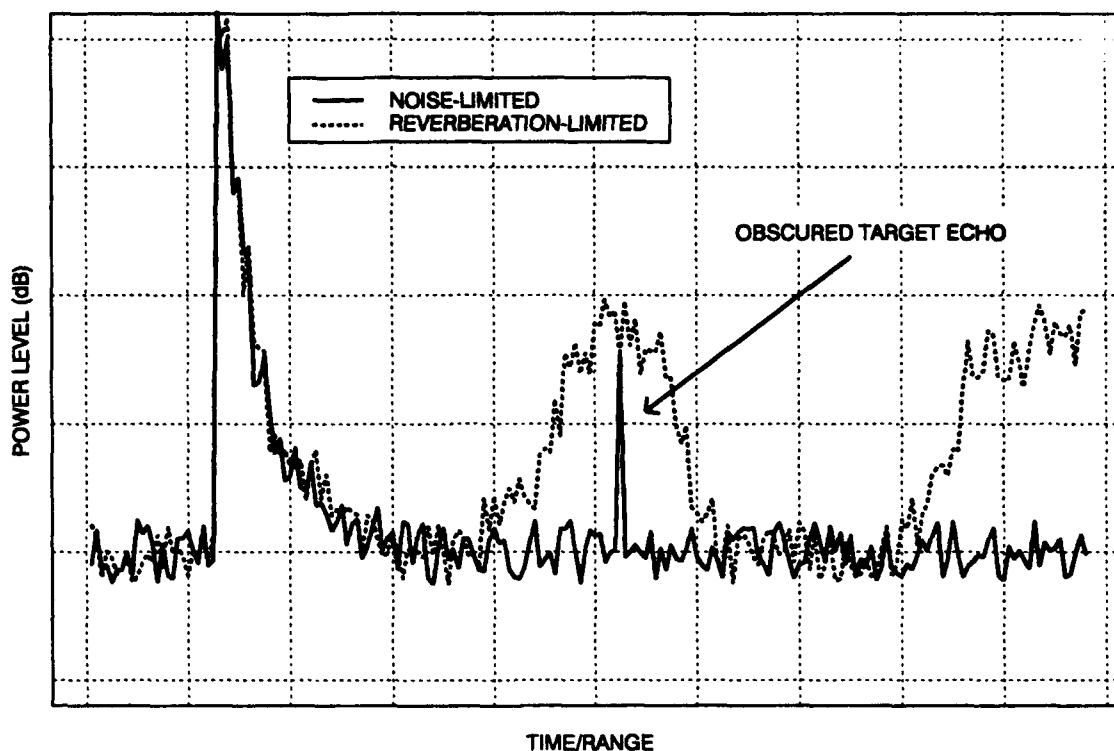


Figure 6. Typical matched filter output, reverberation-limited.

Each individual received ping's matched filter output can be thought of as a single record in a collection or ensemble of records forming the random variable $x_i(t)$. Each ping is aligned in the ensemble so that the beginning of each subsequent record is some multiple of T_{pri} after the beginning of the current record. Done this way, the direct blasts and reverberation features line up. $x_i(t)$ is not ergodic or stationary, in the strictest sense, because the ensemble's mean received power level may vary with time. This is because changing reverberation levels are received through time from reverberation features at different bistatic ranges. However, the statistics for a short localized time window δt , centered at an arbitrary time t' , may be similar between two or more records of the ensemble. For example, the power level may vary similarly through time for one or more records of x_i . This is also shown in figure 7a,b. Assuming similar acoustic propagation conditions, constant source level, and a fixed-fixed geometry, localized reverberation regions of the time series should have similar power levels. Likewise, higher order statistics may also be, in this sense, "stationary" from record to record across the ensemble at a particular time location t' . The interping coherence is a measurement that is made between pairs of records in the ensemble, over the time interval δt . This measurement is made repeatedly at periodic intervals along the time axis, resulting in the interping coherence function. An example of the interping coherence function is shown in figure 7d. From values of interping coherence, the theoretical amount of reverberation reduction can be determined, as will be described in a later section.

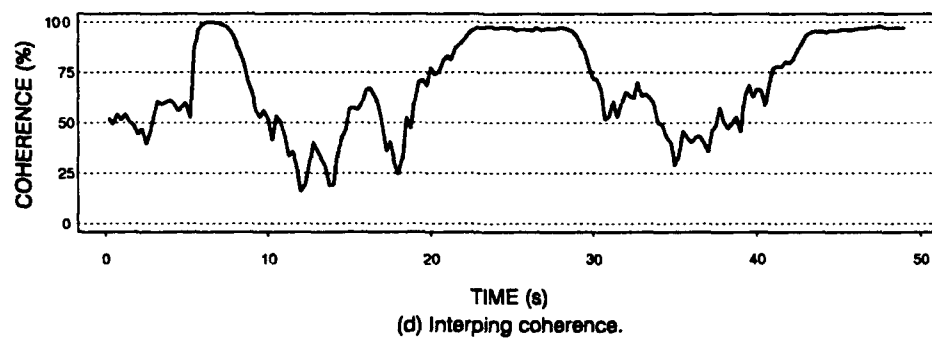
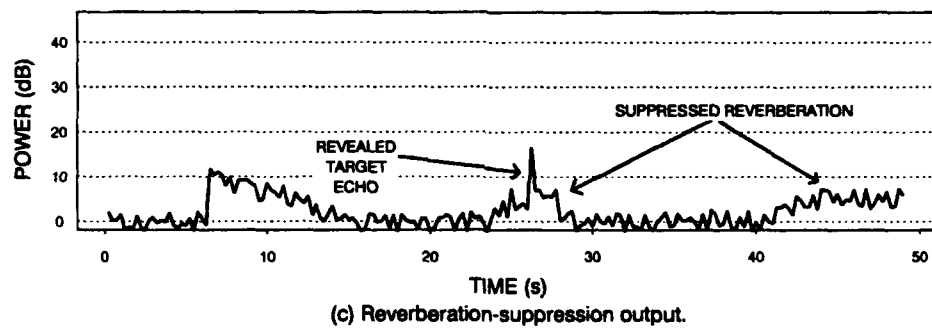
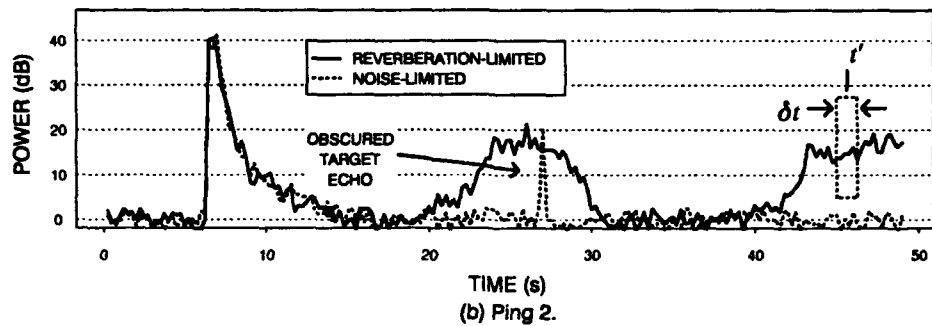
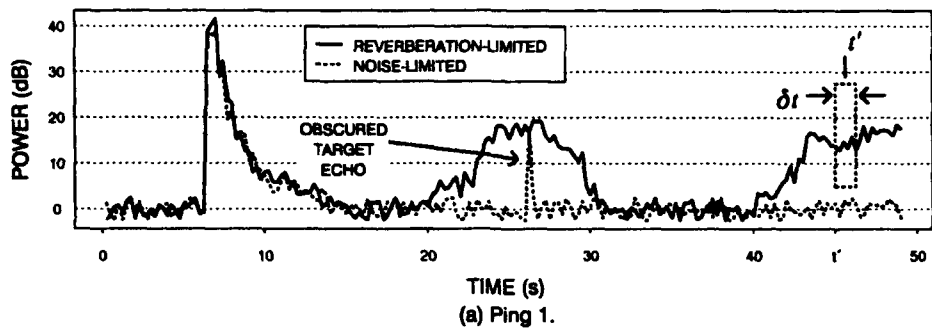


Figure 7. Reverberation processing and interping coherence.

ADAPTIVE REVERBERATION-SUPPRESSION ALGORITHMS

The ping-to-ping subtraction description given is somewhat simplified. Straight coherent subtraction of one ping from another rarely yields the desired output, as shown in figure 7c. This is because the two received signals are not identical, since there may be amplitude variations, time delays, and phase shifts between the reverberation in each of them, as well as a differing local noise component. The actual suppression algorithms are implemented with an adaptive filter structure, so that an optimal estimate is obtained for the reference. Subtraction of this estimate from the input ping yields an output time series with minimum power. The degree to which the adaptive algorithms can do this is determined by the coherence between the two (or more) time series going into the process.

The principles of using an adaptive filter structure for the cancellation of interference, along with some applications in the areas of electrocardiography, speech, and arrays, have been described in detail by Widrow et al.^[3] If a correlated reference of the interference is available, it can be used to obtain an optimum subtraction of the interference in the input. Figure 8 shows a block diagram representing the adaptive filter configuration. The filtered reference signal is subtracted from the input to obtain the output. The goal is to minimize the power of the output signal. To do this, the filter weights are adaptively updated as the data are passed through it, so that the output yields the least possible power. The adaptive weight control mechanism may be one of several types (e.g., least mean square (LMS) and recursive least squares (RLS)); generally it uses prior values of the output to modify the current set of filter weights. In this manner, the feedback loop drives the filter to track the variations in the input data, as well as keep the output power of the filter as small as possible. Figure 8 shows that the reference may be composed as the output of a parallel bank of adaptive filters, each operating on a single reference channel. In this application, the input and the references are obtained from sequentially received pings. Notice that in this configuration, the input ping is not included in the reference, which is referred to as Case 1.

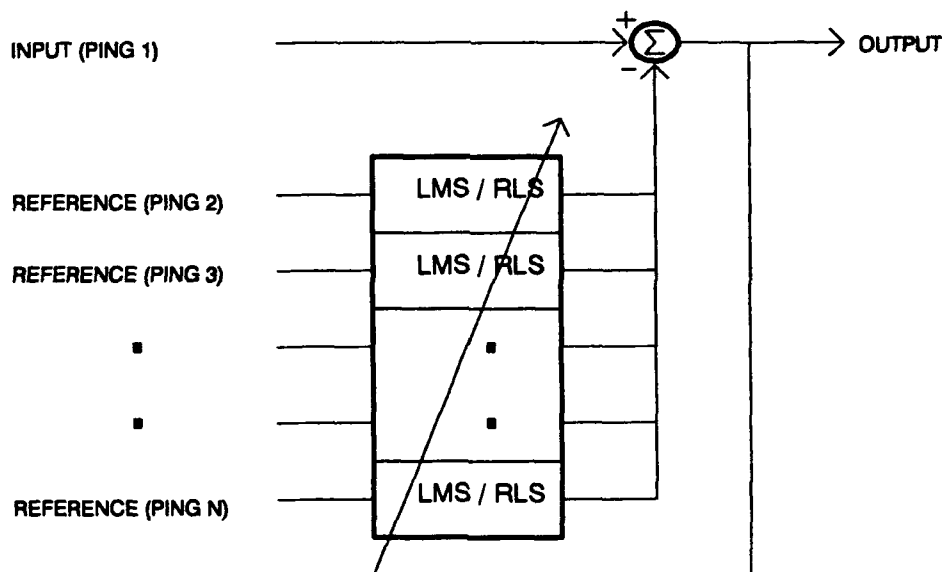


Figure 8. Adaptive suppression using LMS or RLS (Case 1).

There are a variety of algorithms used to adaptively update the filter weights for optimum performance. Detailed descriptions of these algorithms, and their performance characteristics, are given by Haykin, along with an extensive reference list^[4]. Two of the more common algorithms are the LMS and RLS algorithms. Although their goal is the same, the various adaptation schemes perform differently, and one may be better suited to a particular application than others. The differences in the algorithms usually have to do with their tracking performance, their ability to adapt and converge to the optimum filtering solution, and the computational requirements and complexity of the filter implementation.

The adaptive algorithms generally have at least two parameters that must be specified: the adaptation rate or memory and the number of taps in the filter. Although it is not our intent here to discuss the details of these parameters, it is important that appropriate choices of parameters be made, choices that are well suited or matched to the data being processed. One parameter controls the rate at which the adaptive filter will update, in its convergence to the optimal filter solution. It is necessary that the filter adapt fast enough to track the changes in the distributed reverberation to be suppressed, but not so fast that it also removes the target echo. In addition, the number of adaptive weights should be selected to achieve optimum performance for the data being processed.

Figure 9 shows an alternative approach for multiple ping reverberation suppression. Here, the sequentially received pings are considered to be a rectangular data matrix, with the input ping also included. A singular value decomposition (SVD) is then performed on the data matrix. The SVD is essentially an eigenvalue, eigenvector decomposition of the data matrix. The output of the SVD is an estimate of the input, reconstructed with different eigenvalue-weighted combinations of the eigenvectors. Assuming that the reverberation is coherent from ping to ping, the strongest eigenvector is composed essentially of the reverberation, the principal component to be removed. Therefore, the output of the suppression processing is the input ping with one or more of the strongest eigenvectors removed. Figure 9 shows the case where the output is the input ping with the single strongest eigenvector removed. This technique does not require any input parameters, but at the output there may be some uncertainty as to which eigenvector or eigenvectors to remove. This approach is considered as Case 2, differing from Case 1 because it includes the input ping in the makeup of the reference. It will be shown that while this technique reduces more reverberation than the Case 1 technique, it suffers an additional loss, so that its overall performance against reverberation is equivalent to that of the Case 1 technique.

Because the performance of the adaptive algorithms is sensitive to the accompanying parameters and the particular dataset the algorithm are operating on, a reliable method to assess the theoretical performance gains is desired. Knowing the bounds of performance we can then tune the algorithms' parameters until that bound is approached. The theoretical performance criteria are now discussed.

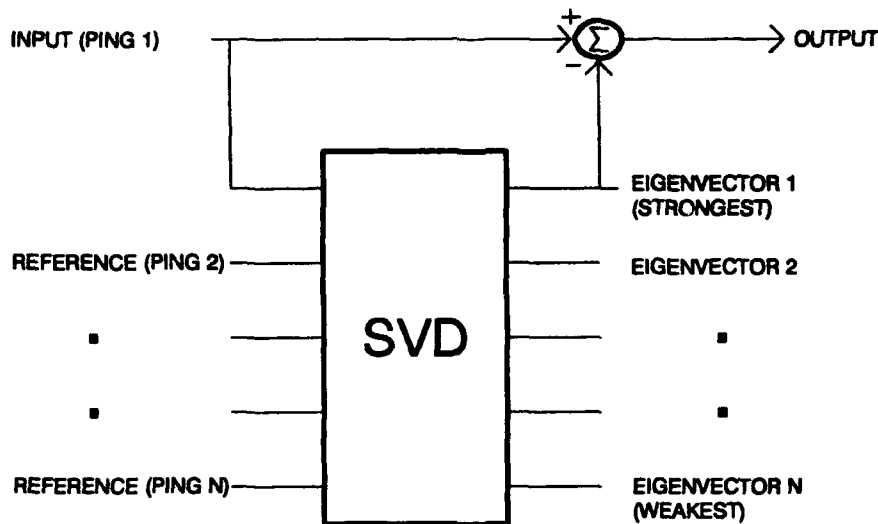


Figure 9. Adaptive suppression using SVD (Case 2).

INTERPING COHERENCE

The normalized cross-correlation function ρ , between two real-valued signals $x_m(t)$ and $x_n(t)$, is given^[5] by the cross-correlation function divided by the power in the two input signals, as

$$\rho_{m,n}(\tau) = \frac{\int_{-\infty}^{\infty} x_m(t) \cdot x_n(t - \tau) dt}{\left[\int_{-\infty}^{\infty} |x_m(t)|^2 dt \cdot \int_{-\infty}^{\infty} |x_n(t)|^2 dt \right]^{1/2}} \quad (5)$$

With this normalized form for correlation, ρ can take on values between -1 and $+1$. Now, consider the case of the two signals x_m and x_n , received from two different transmissions, p_m and p_n . The signals are so aligned by their direct-blast arrival that the reverberation features line up, and a short time window of data, δt , is obtained from each received signal. Using a discrete time implementation, the normalized cross-correlation function is estimated by using the two finite-length segments. Assume that the maximum value of the estimate of $\rho_{m,n}$ occurs at $\tau = \tau_p$, the delay lag at which the two signals are most correlated. The range of lag values for τ is from $-\tau_{max}/2$ to $+\tau_{max}/2$, where τ_{max} may be specified so that bounds are placed on the correlation search, if desired. The interping coherence estimate $\Gamma_{m,n}$ is defined as the absolute value of $\rho_{m,n}$ at the delay $\tau = \tau_p$, such that

$$\Gamma_{m,n} = |\max[\rho_{m,n}(\tau)]| = |\rho_{m,n}(\tau_p)| \quad (6)$$

Here, $\Gamma_{m,n}$ is bounded by 0 and 1 and measures the similarity or coherence between the two signals. This correlation process is then repeated at periodic intervals along the time base of the received pings. Each correlation window overlaps the previous one by a selectable amount, δ_{ol} .

This results in the interping coherence as a function of time, $\Gamma_{m,n}(t)$, which is also dependent on the parameters δt , δ_{ol} , and τ_{max} . This interping coherence function will indicate any regions in range where the reverberation is similar from ping to ping.

Now, consider the interping coherence measurements for a single time window, δt , in terms of the reverberation and noise that make up each signal. For finite-length discrete signals, the correlation integral is a time-averaged product, which is denoted by the symbol $\langle \rangle$. In addition, real-valued signals are considered, and the time dependence is assumed and dropped for simplicity in notation. The following assumptions are made:

1. Each received ping, x_m and x_n , is comprised of a reverberation component and a local ambient noise component as

$$x_m = r_m + n_m, \quad x_n = r_n + n_n \quad (7)$$

2. The reverberation components in the m^{th} and n^{th} pings are identical, perfectly coherent, and given by r_c . In addition, the coherent power, P_C , is given by the averaged square of the reverberation component:

$$\begin{aligned} r_m &= r_n = r_c \\ P_C &= \langle r_c^2 \rangle \end{aligned} \quad (8)$$

3. The coherent reverberation component, r_c , is uncorrelated with the ambient noise in each ping so that their averaged product is zero:

$$\langle r_c \cdot n_m \rangle = \langle r_c \cdot n_n \rangle = 0 \quad (9)$$

4. The noise process in each signal is random, white over the signal frequency band, and uncorrelated with each other. In addition, the averaged noise power, P_N , is assumed to be the same in each signal:

$$\begin{aligned} \langle n_m \cdot n_n \rangle &= 0 \\ \langle n_m^2 \rangle &= \langle n_n^2 \rangle = \langle n^2 \rangle = P_N \end{aligned} \quad (10)$$

5. The interping coherence is equivalent between all pairs of pings going into the reverberation-suppression processing:

$$\Gamma_{m,n} = \Gamma \quad (11)$$

for all interping combinations m, n .

If these foregoing assumptions are made, the interping coherence may be described in term of the reverberation and noise power, as follows: The interping coherence between the m^{th} and n^{th} pings will then be given as

$$\begin{aligned} \Gamma_{m,n} &= \frac{\langle x_m \cdot x_n \rangle}{\sqrt{\langle x_m^2 \rangle \cdot \langle x_n^2 \rangle}} = \frac{\langle (r_c + n_m) \cdot (r_c + n_n) \rangle}{\sqrt{\langle (r_c + n_m)^2 \rangle \cdot \langle (r_c + n_n)^2 \rangle}} \\ &= \frac{\langle r_c^2 + r_c n_m + r_c n_n + n_m n_n \rangle}{\sqrt{\langle r_c^2 + 2r_c n_m + n_m^2 \rangle \cdot \langle r_c^2 + 2r_c n_n + n_n^2 \rangle}} \end{aligned} \quad (12)$$

If assumptions 2, 3, and 4 are made, the reverberation and noise cross-terms are zero, so that the interping coherence simplifies to

$$\Gamma_{m,n} = \frac{\langle r_c^2 \rangle}{\sqrt{\langle r_c^2 + n_m^2 \rangle \cdot \langle r_c^2 + n_n^2 \rangle}} = \frac{\langle r_c^2 \rangle}{\langle r_c^2 + n^2 \rangle} = \frac{P_C}{P_C + P_N} = \frac{P_C}{P_T} \quad (13)$$

where P_C is the power of the coherent reverberation component, P_N is the noise power, and P_T is the total power of both. Therefore, the interping coherence is equal to the ratio of the coherent reverberation power to the total power in the received ping. As the power of the noise increases, the interping coherence decreases, and as the noise decreases, the coherence improves. The interping coherence function may be estimated by measurement, as in Eq. 6. This measurement can be made for every pair of pings going into the process. An example of the interping coherence function for two pings is depicted in figure 7d. In reality, for the noise-only regions, the estimated coherence function does not drop to zero as the expression for coherence predicts. This is because there may be some small correlation due to the finite length of the data going into the estimation of the correlation. Because of this, the estimation of the coherence function may exhibit a slightly higher floor than that for a completely uncorrelated signal. In addition, the cross-correlation function has freedom to search over some range in τ for possible correlations. Hence, although the noise signals are uncorrelated, there may be some significant nonzero correlation at other delays, which is picked as the peak. In any case, the levels are typically still smaller than 0.5 for appropriate choices of τ_{max} .

Finally, the power of the coherent reverberation component can be expressed as a function of the noise power and the interping coherence from Eq. 13 as

$$P_C = \frac{P_N \cdot \Gamma}{1 - \Gamma} \quad (14)$$

From these results, expressions can be obtained for the theoretical amount of reverberation that may be reduced. Two cases are considered. In Case 1, the reference ping to be subtracted is made up of one or more pings other than the input ping. In Case 2, the input ping itself is included in the formulation of the reference. When all suppression gains and echo losses are taken into account, the performances of Case 1 and Case 2 implementations are equivalent, when the same number of pings are used. It will be shown that while Case 2 suppresses more reverberation than Case 1, it also suffers an additional loss in target echo level, so that its overall performance is equivalent.

REVERBERATION POWER REDUCTION (CASE 1)

Consider the reverberation subtraction process as depicted in figure 8. A total of N pings are to be used in the reverberation-suppression processing. One of the pings is chosen as the input ping, and the remaining pings are used in the formulation of the reference ping. When the input ping is not included, the reference may be modeled as the average of M pings, where $M = N - 1$. The output of the suppression processing, y , is the reference subtracted from the input as

$$y = x_{input} - x_{ref} \quad (15)$$

The reference ping is modeled as the average of M pings so that

$$x_{ref} = \frac{1}{M} \sum_{i=1}^M x_i = r_c + \frac{1}{M} \sum_{i=1}^M n_i \quad (16)$$

Now, from Eq. 15 and 16, the output is given by

$$\begin{aligned} y &= (r_c + n_{input}) - r_c - \frac{1}{M} \sum_{i=1}^M n_i \\ &= n_{input} - \frac{1}{M} \sum_{i=1}^M n_i \end{aligned} \quad (17)$$

Detection processing is done on the output power of the data. The output power, P_y , is obtained by squaring the output signal as

$$P_y = \langle y^2 \rangle = n^2 + \frac{1}{M} n^2 = P_N \left(1 + \frac{1}{M} \right) \quad (18)$$

For a simple two ping subtraction case ($M = 1$), the output power reduces to twice the noise power of the input.

Now, from Eq. 14 and 18, the reverberation processing power gain for this case, α_1 , can be obtained. The gain is the ratio of output power to input power as

$$\begin{aligned} \alpha_1 &= \frac{P_y}{P_x} = \frac{\left(1 + \frac{1}{M}\right)P_N}{P_C + P_N} = \frac{\left(1 + \frac{1}{M}\right)P_N}{\left(\frac{\Gamma}{1-\Gamma}\right)P_N + P_N} \\ &= \frac{(M+1) \cdot (1-\Gamma)}{M} = \frac{N(1-\Gamma)}{(N-1)} \end{aligned} \quad (19)$$

The reciprocal of the power gain gives the reverberation power reduction (RPR), defined for Case 1 as

$$RPR_1 = 10 \log_{10} \left(\frac{1}{\alpha_1} \right) = 10 \log_{10} \left[\frac{(N-1)}{N(1-\Gamma)} \right] \quad (20)$$

Equation 20 gives the theoretical amount of reverberation power (in decibels) that is reducible, as a function of the interping coherence. As the measured interping coherence increases, the RPR increases. Figure 7c depicts the power output of a two-ping subtraction. Notice how areas of large reduction in reverberation correspond to areas of high interping coherence.

Figure 10 shows theoretical plots of RPR_1 as a function of Γ , for three different values of N . Notice that while the RPR may take on negative values for small values of interping coherence, only the positive portions are plotted. This is the applicable region of the curves, since the adaptive algorithms do not yield output power greater than the amount in the input. It can be seen that as more pings are used in the reference, greater reductions are obtained against reverberation, for a fixed coherence value. The upper bound of reduction is shown for $N = \infty$, which is a constant 3 dB above the $N = 2$ case, for any given coherence value. For the same suppression level, the multiple-ping reference does not require values of Γ to be as high, particularly at smaller RPR levels. It is also seen that large reductions in reverberation require a high degree of interping coherence. The $N = 2$ case requires values of coherence greater than 0.5 to achieve any reverberation reduction at all.

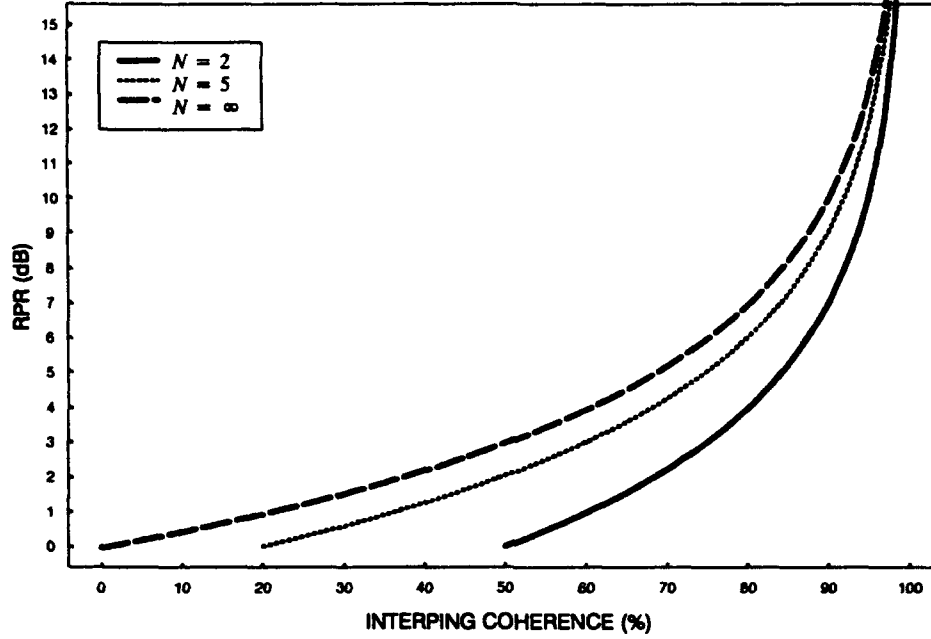


Figure 10. Theoretical RPR_1 vs. interping coherence.

REVERBERATION POWER REDUCTION (CASE 2)

In Case 2, the input signal is included in the formulation of the reference signal. This is the case for a sequence of pings input into an SVD algorithm, as shown in figure 9. Again, assume that a total of N pings are used in the reverberation processing and that one of the pings is chosen as the input ping. Here, the reference is considered to be an average of the total of all N pings, including the input, such that

$$x_{ref} = \frac{1}{N} \sum_{i=1}^N x_i = r_c + \frac{n_{input}}{N} + \frac{1}{N} \sum_{i=1}^{N-1} n_i \quad (21)$$

where the input ping is taken outside of the summation. As before, the output is obtained by subtracting the reference from the input ping as

$$\begin{aligned} y &= \left(r_c + n_{input} \right) - r_c - \frac{n_{input}}{N} - \frac{1}{N} \sum_{i=1}^{N-1} n_i \\ &= \left(\frac{N-1}{N} \right) \cdot n_{input} - \frac{1}{N} \sum_{i=1}^{N-1} n_i \end{aligned} \quad (22)$$

The output power of the suppression processing is obtained by squaring the output signal as

$$P_y = \langle y^2 \rangle = \left[\left(\frac{N-1}{N} \right)^2 + \frac{(N-1)}{N^2} \right] P_N = \frac{(N-1)}{N} P_N \quad (23)$$

Comparing this result with Case 1 (Eq. 18) shows a reciprocal relationship between the factors $(N-1)/N$ and $(M+1)/M$ multiplying P_N . This is because in this case, the input is included in the reference, whereas in Case 1, it is not. Consequently, the output power for Case 2 will always be

smaller than for Case 1 for the same choice of N , with less difference as N increases. As before, the suppression gain is the ratio of output power to input power, given in this case by

$$\alpha_2 = \frac{P_y}{P_x} = \frac{\left[\frac{(N-1)}{N}\right]P_N}{\left(\frac{\Gamma}{1-\Gamma}\right)P_N + P_N} = \frac{(N-1) \cdot (1-\Gamma)}{N} \quad (24)$$

The reverberation power reduction for Case 2 is given by

$$RPR_2 = 10 \log_{10}\left(\frac{1}{\alpha_2}\right) = 10 \log_{10}\left[\frac{N}{(N-1)(1-\Gamma)}\right] \quad (25)$$

Plots of RPR_2 are shown in figure 11. Here, compared with Case 1, higher levels of reverberation reduction are possible. While this is indeed true, it is somewhat misleading, as this method also yields a reduction in target echo level. This is due to the fact that the target echo in the input ping is also a part of the reference and therefore partially subtracts itself out. This is the reference loss (RL), which only applies to Case 2 implementations, and it is discussed in more detail in a subsequent section. Notice the reciprocal nature of the curves relative to Case 1. The upper bound occurs for $N = 2$, and the lower bound is when $N = \infty$. Also notice that for $N = \infty$, $RPR_1 = RPR_2$.

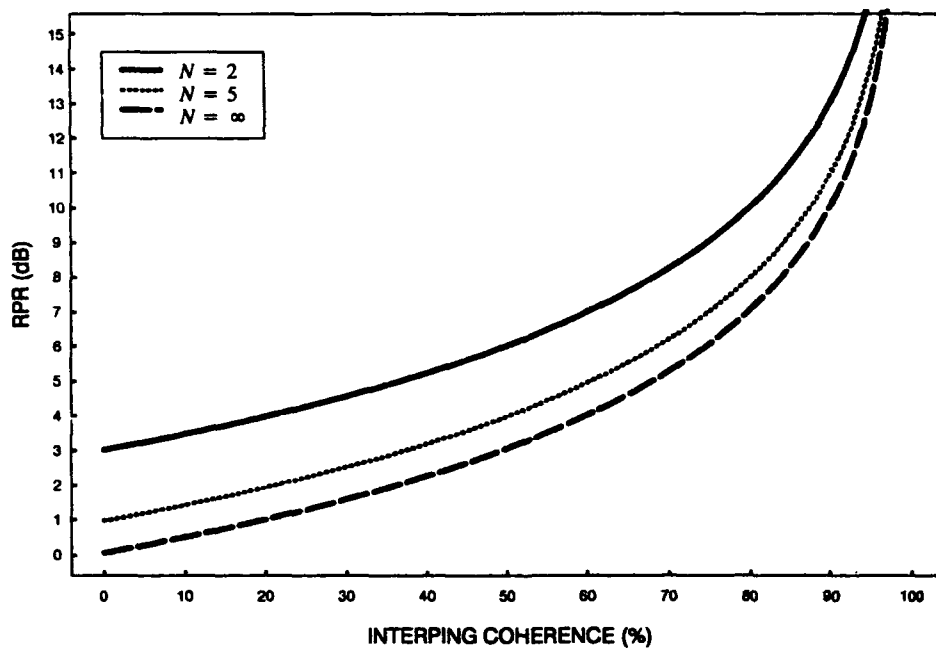


Figure 11. Theoretical RPR_2 vs. interping coherence.

COHERENCE OF REVERBERATION

The interping coherence has been described based on the assumption that the reverberation is perfectly coherent between the pings used in the process. In reality, this may not be so in many acoustic environments. In addition to the decrease in interping coherence due to uncorrelated noise, there may also be some decrease due to reverberation that is only partially coherent. This

effect, along with the impact of the input ping's reverberation-plus-noise-to-noise-power ratio (RNNR), is now explained. The RNNR can be expressed as

$$RNNR = \frac{P_C + P_N}{P_N} = \frac{P_T}{P_N} \quad (26)$$

where the assumptions made for interping coherence previously still apply. This quantity can be estimated by measuring the total received power and dividing by an estimate of the noise power. The noise power estimate may be obtained from the received data stream just before active transmissions or by measuring the noise power in an adjacent frequency band just outside the transmitted signal. The RNNR is important because it indicates whether the data are noise-limited or reverberation-limited. For a reverberation-limited case, $P_C > P_N$, and the RNNR is greater than 3 dB. For a noise-limited case, $P_C < P_N$, and the RNNR is less than 3 dB. When no reverberation is present (noise-only case), $P_C = 0$, and the $RNNR = 0$ dB.

Assuming a perfectly coherent reverberation component, the maximum possible values of the interping coherence can be determined by measuring or estimating the RNNR. Assume that before the start of any transmissions, the average ambient noise power level is P_{Namb} , and that it remains constant. Once the transmissions have begun, the received signal power is the sum of the reverberation power, P_C , and the noise power. The maximum value that Γ can achieve, based on the RNNR, can be obtained with estimates of total received power and noise power as

$$\Gamma_{max} = \frac{P_T - P_{Namb}}{P_T} = 1 - \frac{1}{RNNR} \quad (27)$$

The maximum interping coherence is shown in figure 12, as a function of the input's RNNR. It is clear from this figure that as the reverberation level drops relative to the noise, the maximum interping coherence drops, resulting in less suppression performance. But because there is less reverberation in the input, there is less reverberation power to suppress. If the assumptions outlined in the Interping Coherence section are indeed true, then the measured interping coherence will be equal to this maximum coherence level. In that case, the interping coherence is only a function of the input RNNR.

Now, consider the case where the reverberation component is not perfectly coherent such that

$$r_m \neq r_n \neq r_c \quad (28)$$

Considering only the reverberation component, in the absence of noise, the coherence for reverberation is

$$\Gamma_{reverb} = \frac{\langle r_m \cdot r_n \rangle}{\sqrt{\langle r_m^2 \rangle \cdot \langle r_n^2 \rangle}} \quad (29)$$

The interping coherence that is measured using cross-correlation is bounded by the maximum coherence and reduced by the coherence of the reverberation component, as

$$\Gamma = \Gamma_{reverb} \cdot \Gamma_{max} \quad (30)$$

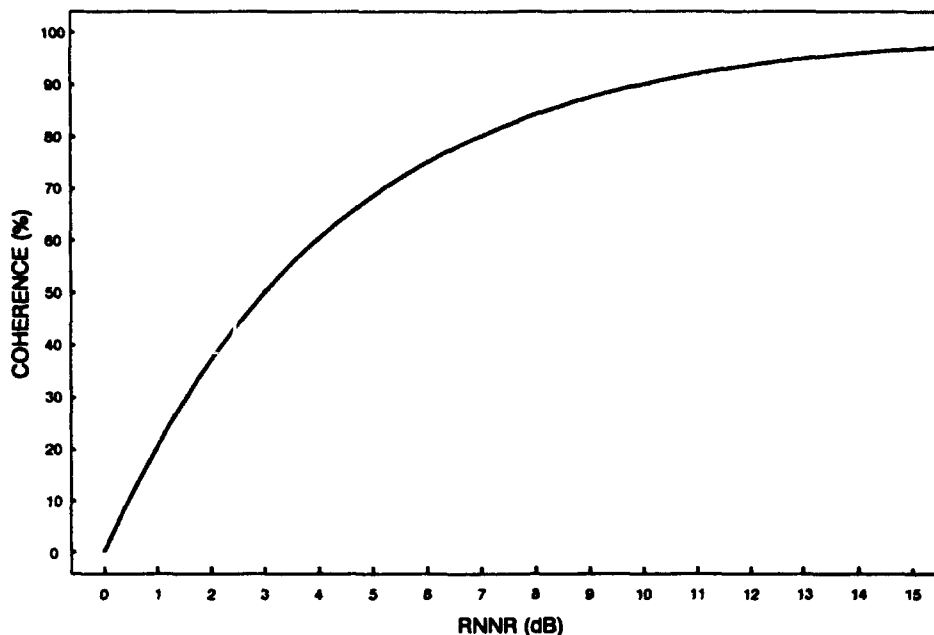


Figure 12. Maximum coherence obtainable vs. RNNR.

Figure 13 shows curves of the RPR_1 ($N = 2$) obtainable as a function of input RNNR for various values of Γ_{reverb} . Notice that at high RNNRs, the RPR is decreased significantly as the coherence of the reverberation component is decreased only slightly. Again, as before, the plot only shows the curves for positive RPRs, since the algorithms do not allow output power to exceed input power. Notice that in this case, no gains can be made if the RNNR is less than 3 dB. This means that only when $P_C > P_N$ are any gains made for a two-ping suppression process. Also, the uppermost curve ($\Gamma_{reverb} = 1.0$) shows that even with the maximum amount of coherence in the reverberation component, there is still a residual RNNR of 3 dB after suppression. This implies that no reductions of reverberation power, P_C , are possible below the power of the noise, P_N , for a two-ping process. The coherence of the reverberation can be estimated by measuring the interping coherence function and dividing by the estimate of Γ_{max} in Eq. 27. Γ_{max} may be estimated by measuring the total power and the power of the noise as described. In this manner, the coherence of the received reverberation component can be estimated.

Figure 14 shows a similar set of curves for Case 2, with five pings going into the process. Here, with multiple pings used, there is an increase in reverberation suppression for all values of Γ_{reverb} . Still, as before, the suppression drops as the coherence of reverberation decreases. For $\Gamma_{reverb} = 1$, the RPR is 1 dB larger than the input RNNR. Even for a noise-only case ($RNNR = 0$ dB), with no reverberation present, the input signal is reduced by 1 dB. This is because the input is included in the reference, resulting in additional suppression. It is important to note that in this case, a small loss in both noise and target echo levels will occur. This effect is described in detail in a later section.

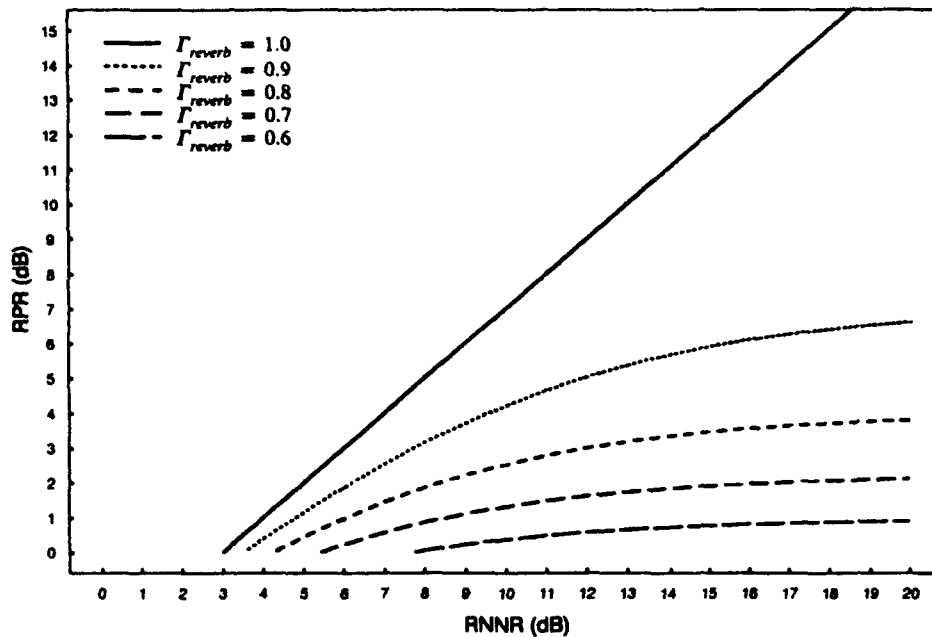


Figure 13. Theoretical RPR_1 vs. input RNNR ($N = 2$).

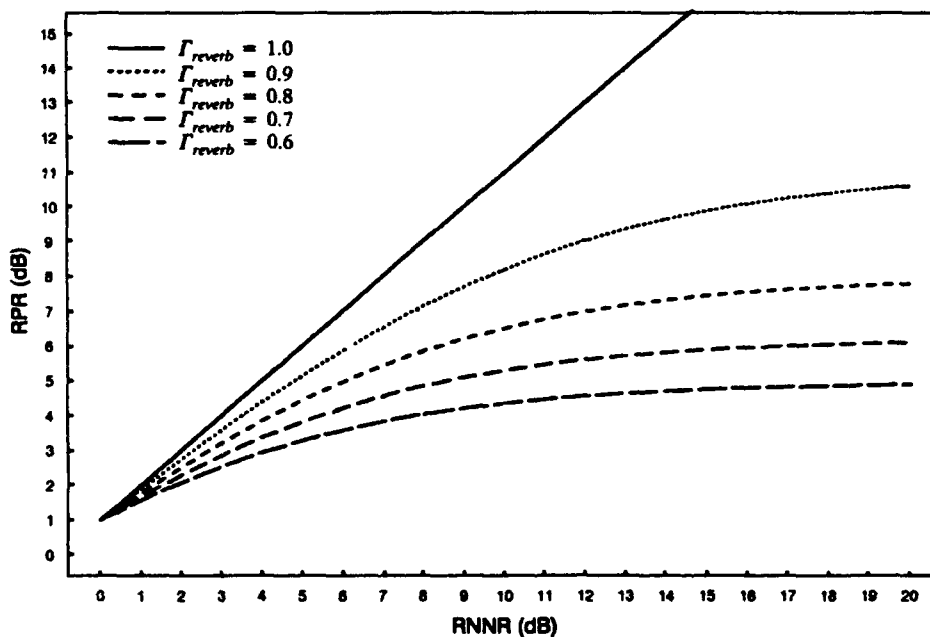


Figure 14. Theoretical RPR_2 vs. input RNNR ($N = 5$).

TARGET ECHO LOSSES

While the ability to suppress reverberation is indeed valuable, it does little good if the target echo is also suppressed or eliminated. Ultimately, the desire is to improve the detectability of the target echo. With this in mind, little loss is tolerated in the target echo level, while as much reverberation is suppressed as possible. In this manner, the target's signal-to-background ratio is

enhanced and the echo becomes more detectable. Now, the theoretical requirements of target motion (Doppler) for echo preservation in the subtraction process will be discussed.

Consider the target's motion relative to the sonar system, as shown in figure 3. The target is assumed traveling with a constant velocity, v_T , and constant heading over the interval of time that reverberation is being processed for suppression. Assume that the source and the receiver are fixed in location, with no motion. The velocity of the target with respect to a bistatic geometry, v , is given^[2] as

$$\begin{aligned} v &= v_T \cdot (\cos \theta_{ts} + \cos \theta_{tr}) \\ &= 2v_T \cdot \cos \theta_{tb} \cdot \cos \frac{\beta}{2} \end{aligned} \quad (31)$$

where θ_{ts} , θ_{tr} , θ_{tb} , and β are various angles associated with the geometry as shown in figure 3. β is defined as the opening angle between the source, target, and receiver. θ_{tb} is the angle from the target heading to the bisector of β and is known as the target bistatic aspect angle. The angles θ_{ts} and θ_{tr} are defined as the angles from the target heading to the source and receiver, respectively. Notice that if β is equal to zero and $d_{st} = d_{tr}$, the system is monostatic, with the source and receiver colocated. In addition, if $\theta_{tb} = 0$, the target is moving radially, with an closing velocity component given by $2v_T$.

Assuming the use of certain broadband signals processed with matched filtering, the Doppler of the received target echo is not observable as a shift in frequency but as a change in range from one ping to the next. This change in bistatic range corresponds to the location of the target at different equitime ellipses from ping to ping. After alignment of the m^{th} and n^{th} pings for subtraction, the time shift between echoes is given by the difference in arrival time relative to their respective direct-blast receptions. The time shift between echoes, Δt_e , is given as

$$\Delta t_e = t_{e_m} - t_{e_n} = \frac{v \cdot \Delta T}{c}, \quad \text{where } \Delta T = (m - n) \cdot T_{pri} \quad (32)$$

Assuming that the received reverberation is caused by scatterers that are stationary, and that it is coherent from ping to ping, it may be suppressed according to the appropriate RPR for the method used. To do this, the parameters of the adaptive filtering algorithm must be so tuned that the algorithm is updating quickly enough to track and cancel the distributed reverberation background, but not so quickly that it cancels uncorrelated random noise. There may or may not be subtraction of the input target echo, depending on the amount of time shift between the echoes from ping to ping after alignment. At the output of the replica correlator, in the absence of noise, the target echo is approximated by the autocorrelation function of a band-limited, flat spectral signal. The frequency modulated chirp waveforms have these frequency characteristics. A real-valued representation of a target echo for these types of waveforms is given^[6] by

$$e(t) \approx \frac{\sin(\pi B t)}{\pi B t} \cdot \cos(2\pi f_c t) = \text{sinc}(\pi B t) \cdot \cos(2\pi f_c t) \quad (33)$$

where f_c and B are the transmitted signal center frequency and bandwidth, respectively. The echo has a carrier frequency which is modulated by a sinc function. Figure 15 shows an example of a noise-free echo signal at the output of the correlator with the ratio of center frequency to bandwidth equal to 3.33. The maximum peak of the target echo that stands up above the background level provides the target's detectability. Therefore, the observable echo level at the output, e_{out} , is the maximum of the difference between two identical echoes, one shifted relative to the other, as

$$\begin{aligned}
e_{out} &= \text{MAX}\{e_m(t) - e_n(t - \Delta t_e)\} \\
&= \text{MAX}\left\{ \text{sinc}(\pi B t) \cdot \cos(2\pi f_c t) \right. \\
&\quad \left. - \text{sinc}\left[\pi B\left(t - \frac{v\Delta T}{c}\right)\right] \cdot \cos\left[2\pi f_c\left(t - \frac{v\Delta T}{c}\right)\right] \right\} \quad (34)
\end{aligned}$$

The input echo level, e_{input} , is the maximum of the single target echo in the input time series which in this case is equal to one. The echo loss (EL), which is the loss in echo power can then be given by the ratio of input to output levels as

$$EL = 10 \log_{10}\left(\left|\frac{e_{input}}{e_{out}}\right|^2\right) = 10 \log_{10}\left(\left|\frac{1}{e_{out}}\right|^2\right) \quad (35)$$

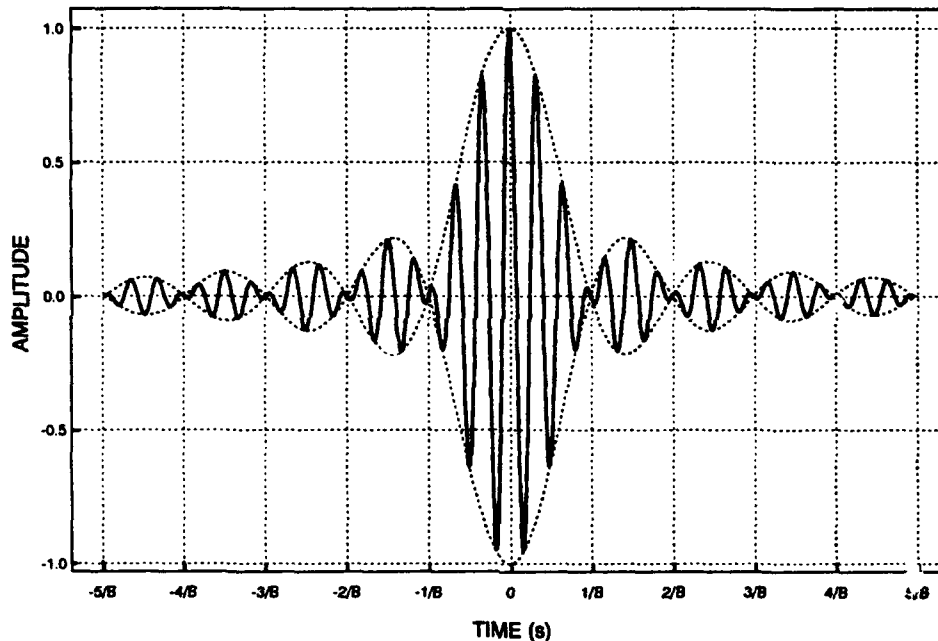


Figure 15. Modulated sinc function ($f_c/B = 3.33$).

Figures 16 through 19 show four plots of EL, shown as a function of echo time shift, Δt_e , for waveform center-frequency-to-bandwidth ratios of $f_c/B = 1.67, 3.33, 6.67,$ and 13.33 . Observe that the output echo power oscillates at the carrier frequency, f_c , but is bounded by an upper and a lower envelope. Depending on the echo's time shift, the output echo power can undergo significant enhancement or cancellation, particularly at small shifts. For values of echo time shift less than $1/B$, severe cancellation and significant enhancements are realizable. The echo levels in this region are highly unpredictable and therefore deemed unreliable. Clearly, as the echo time shift increases beyond $1/B$, there are still enhancement and cancellation peaks, yet the excursions from the input echo level (0 dB) are reduced, as they attenuate with increasing shift. If, the target motion is such that it yields an echo shift that is in this region, the target echo will be reliably preserved.

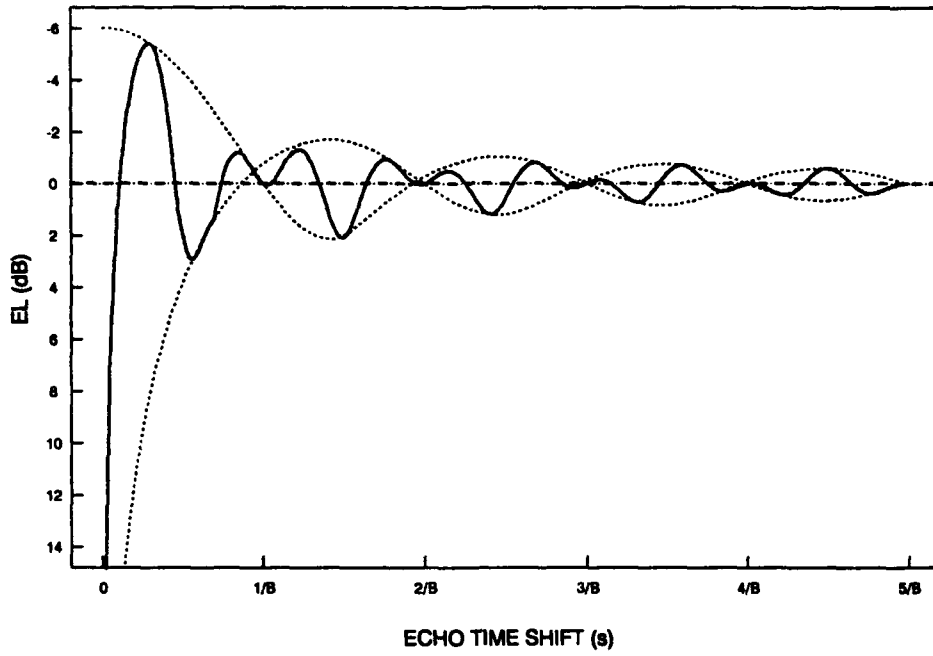


Figure 16. Echo loss vs. echo time shift ($f_c/B = 1.67$).

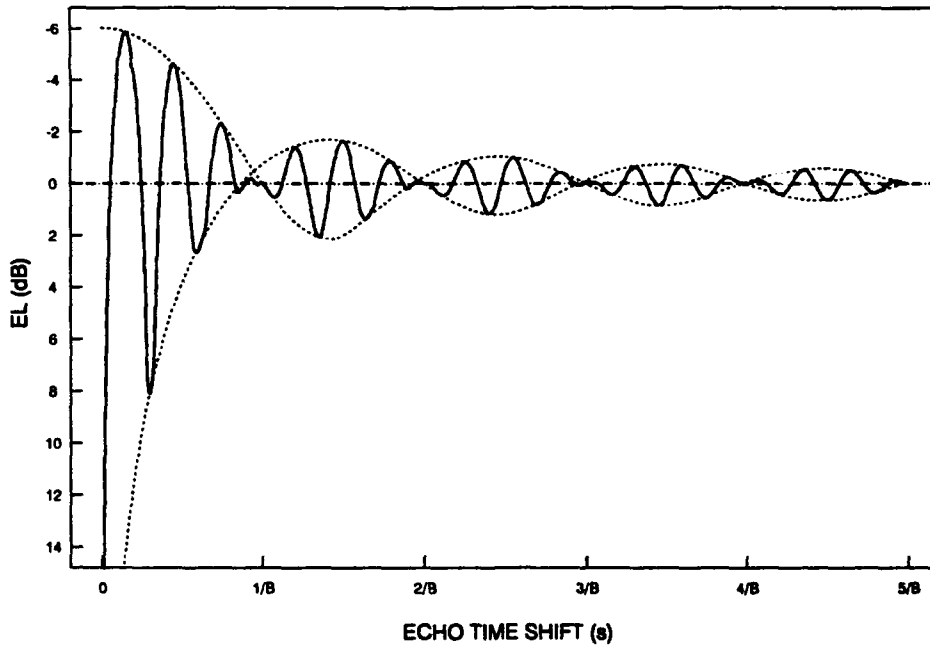


Figure 17. Echo loss vs. echo time shift ($f_c/B = 3.33$).

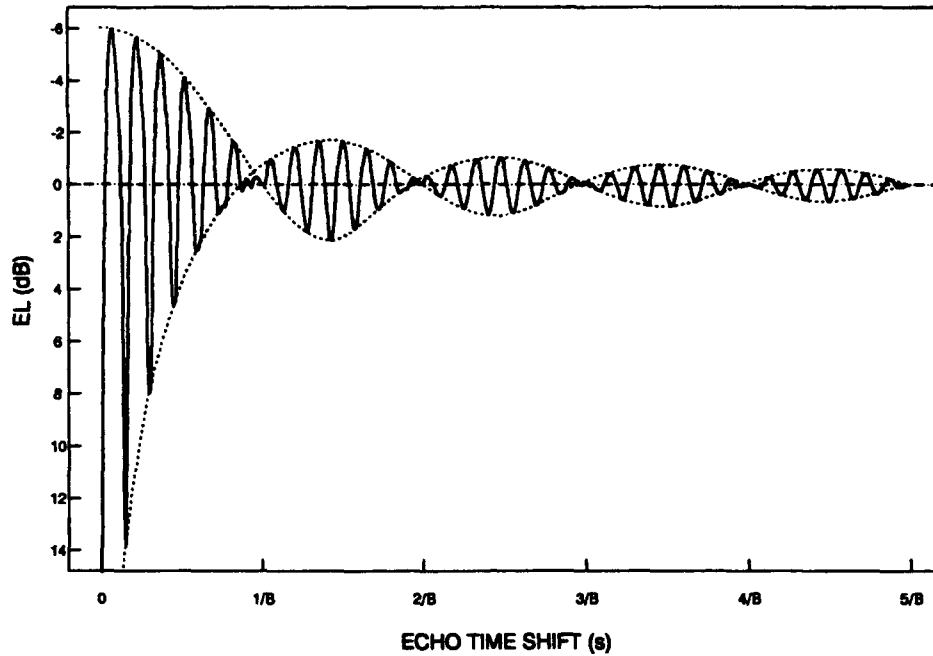


Figure 18. Echo loss vs. echo time shift ($f_c/B = 6.67$).

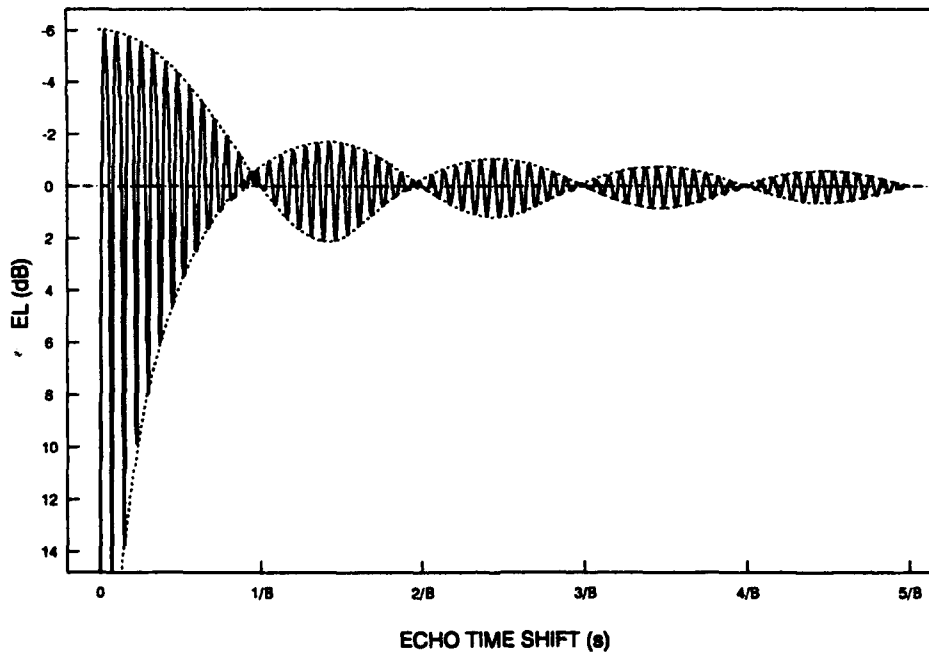


Figure 19. Echo loss vs. echo time shift ($f_c/B = 13.33$).

In order to validate that these curves accurately reflect the behavior of the echo loss, target echoes were synthesized and a simulation was performed. For this simulation, two time series (pings) were produced with an identical random noise signal, in order to model a perfectly coherent reverberation background. A hyperbolic-frequency modulated (HFM) waveform was then added to each of the two time series, as a simulation of the echo. The echo waveforms had a

selectable Doppler shift applied to them before they were summed with the reverberation. This Doppler shift was determined by specifying both the bistatic velocity and the ping repetition interval, as in Eq. 32. The simulated echoes were given such large negative signal-to-background levels that they were deeply buried in and obscured by the simulated reverberation. The two time series were then matched-filtered with a replica of the HFM waveform. Even with the resultant gain of the matched filter, the target echoes were still obscured by the reverberation.

A subtraction algorithm was then applied to the two time series and the output echo levels were measured from the suppression output. In this manner, the echo loss was measured for a particular Doppler assumption. This procedure was then repeated many times, with a large set of different Doppler assumptions, in order to trace EL as a function of target Doppler. Figure 20 shows the echo loss measurements for a set of 400 subtractions with different Doppler assumptions. For this simulation, the ping repetition interval was set at 60 seconds, while the bistatic velocity was varied over the range from 0 to 6 knots, so that the echo time shift is only a function of the target velocity. The embedded target echo waveform had a center-frequency-to-bandwidth ratio of 3.33. Here, a straight coherent (nonadaptive) subtraction was performed. It is clear that the simulation of echo loss agrees very closely with what is predicted by the theory (Eq. 34 and 35). Next, the simulation was performed using the adaptive RLS filter for the subtraction. Figure 21 shows the result of this echo loss simulation over the same range of velocities as before. Here again, that the simulated echo loss is behaving as predicted by theory. Also, that the measured echo loss of the RLS simulation is virtually identical to the simulation of the nonadaptive subtraction. The results of this simulation indicate that the theoretical echo loss given in Eq. 34 and 35 is an accurate predictor of the type of echo losses that will be suffered with real target echo data.

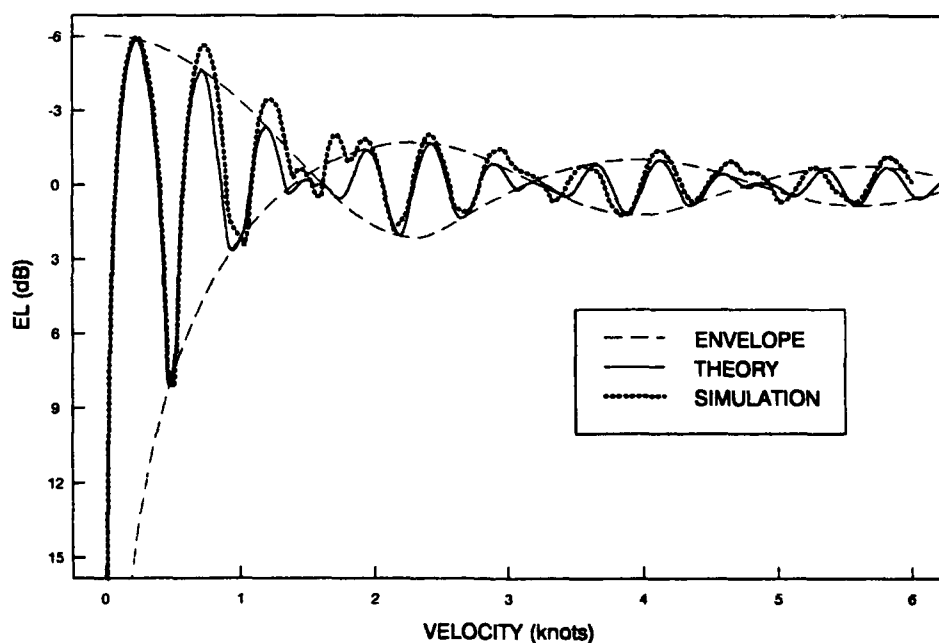


Figure 20. Echo loss, theory vs. simulation (nonadaptive).

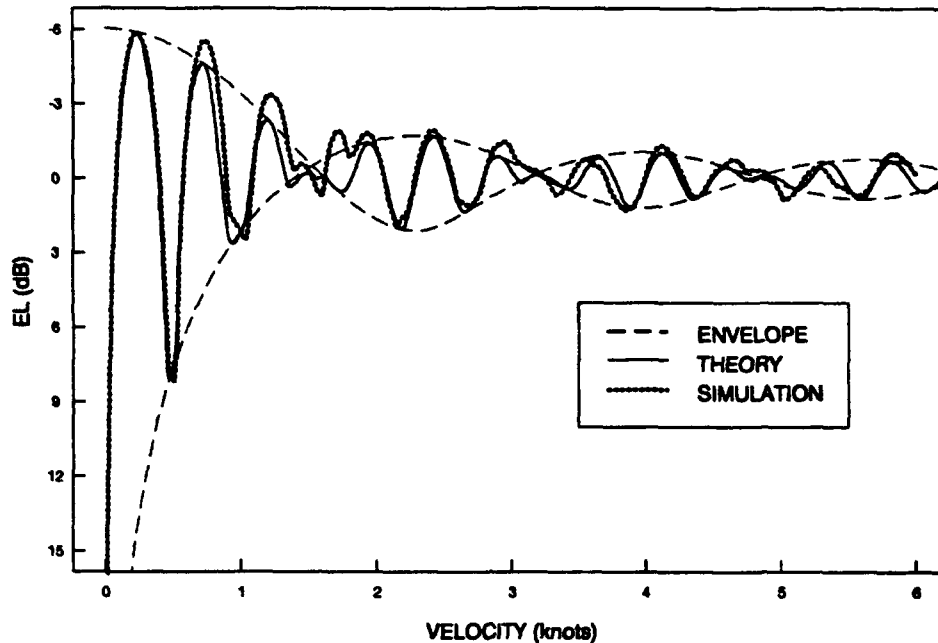


Figure 21. Echo loss, theory vs. simulation (RLS).

Now consider only the two bounding envelopes, which determine the regions of echo shift for reliable target preservation. The envelopes themselves are solely a function of the transmitted pulse bandwidth. Figures 22 through 25 show both envelopes for values of $B = 10, 20, 30,$ and 40 Hz, respectively. Notice that as the bandwidth increases, the envelopes attenuate much earlier. Therefore, increases in bandwidth allow for searches of targets with smaller Doppler shifts, as the reliable target preservation region extends down to slower velocities.

Now consider a specific example of EL as shown in figure 26. The time shift is composed of the velocity component and the time between pings. Here the bandwidth is equal to 30 Hz, and the horizontal axis is the radial velocity component, v , of the target in knots. Several sets of envelopes are shown overlaid, for different values of time between pings, ΔT . As ΔT is lengthened, the reliable region for echo preservation is extended down to slower Doppler shifts.

Figure 27 shows a similar plot for different target velocities. Here, for a fixed time between pings, faster moving targets are the most reliably detected. These plots aid in the determination of the range of target Doppler shifts that will be passed through the subtraction with minimum loss. In addition, they facilitate the determination of optimum values of ΔT for detection in certain target-motion scenarios. While it is desirable to extend ΔT to obtain reverberation suppression for slow targets, there may be limits to how much this can be done. It is vital that the interping coherence remain high over the time period considered. For some acoustic environments, the reverberation field may only be stationary over some finite length interval of time. In such an event, the interping coherence may decrease in level as ΔT is increased beyond this time interval, lowering the obtainable RPR.

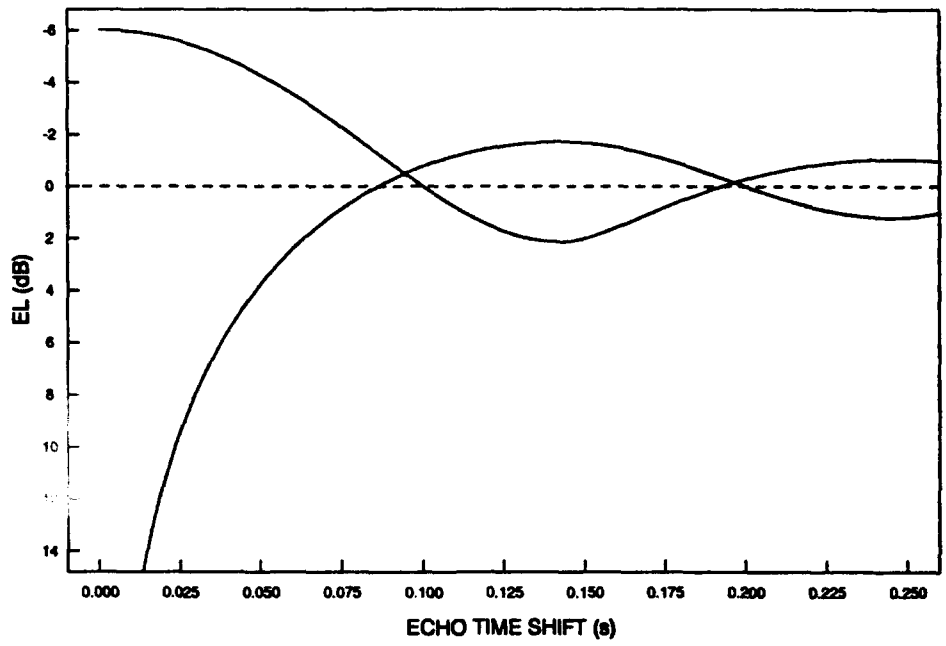


Figure 22. Echo loss envelopes ($B = 10$).

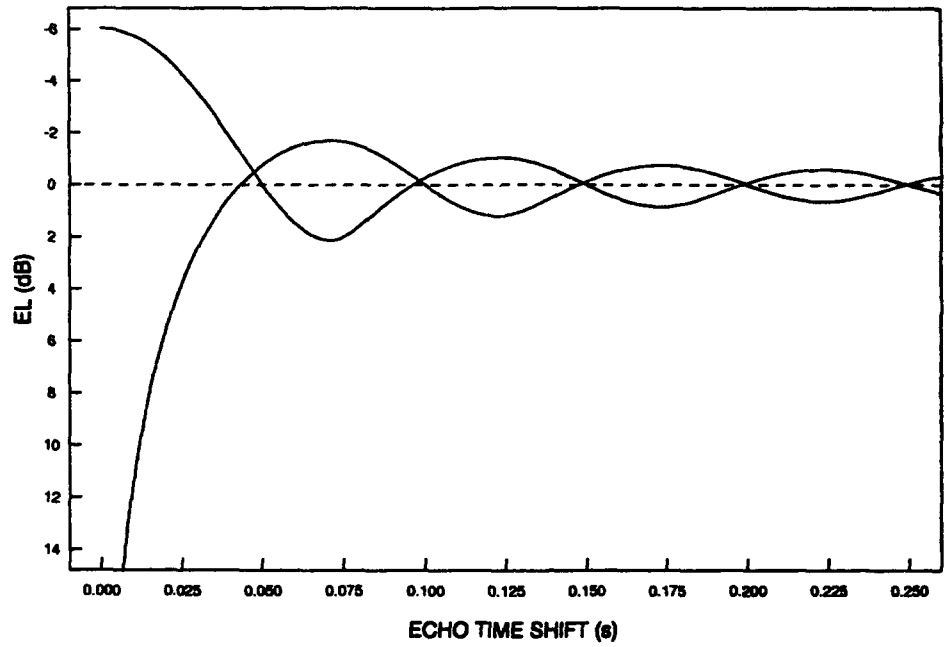


Figure 23. Echo loss envelopes ($B = 20$).

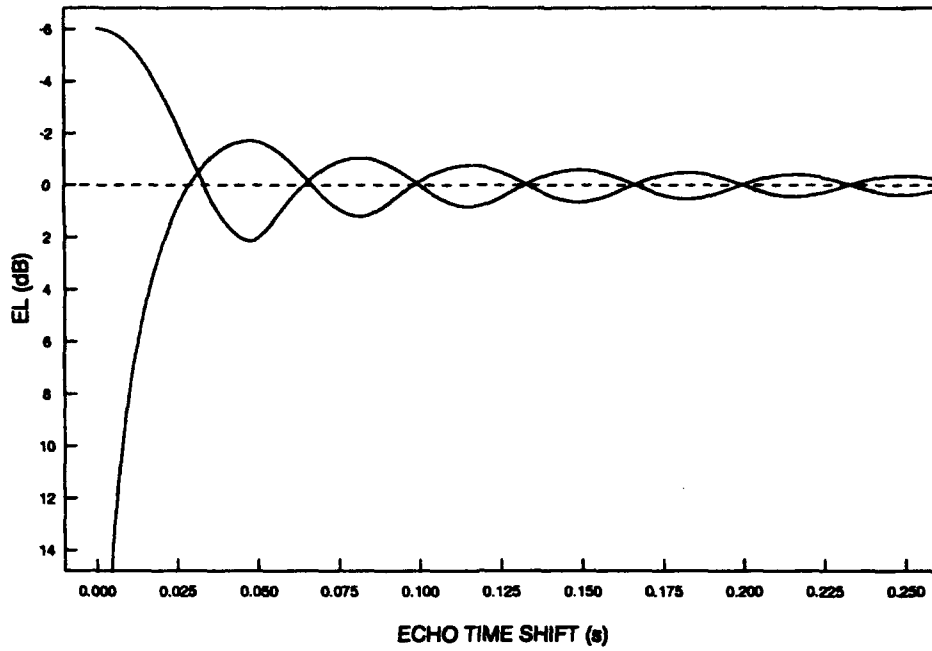


Figure 24. Echo loss envelopes ($B = 30$).

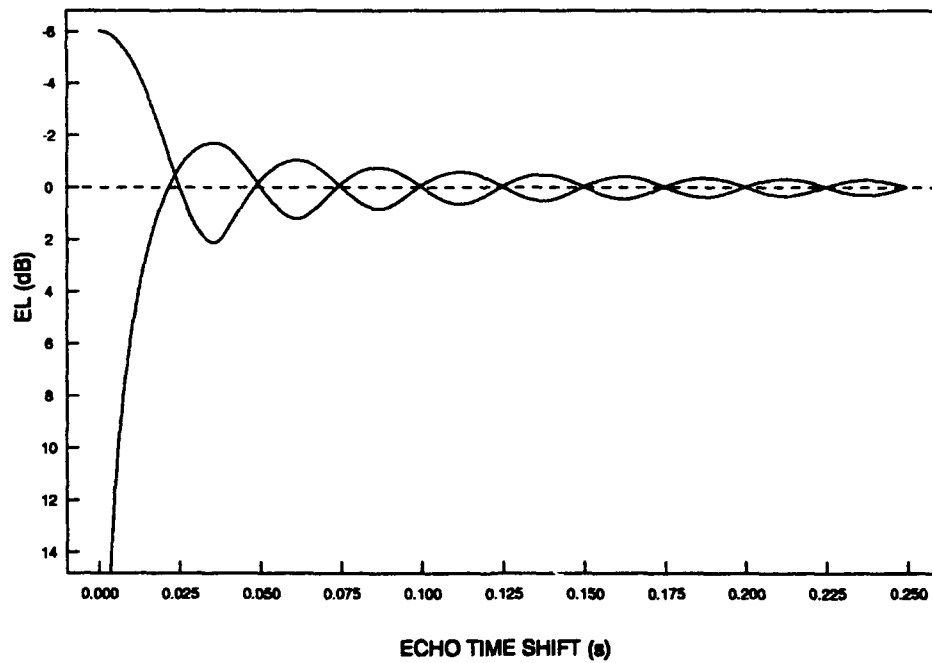


Figure 25. Echo loss envelopes ($B = 40$).

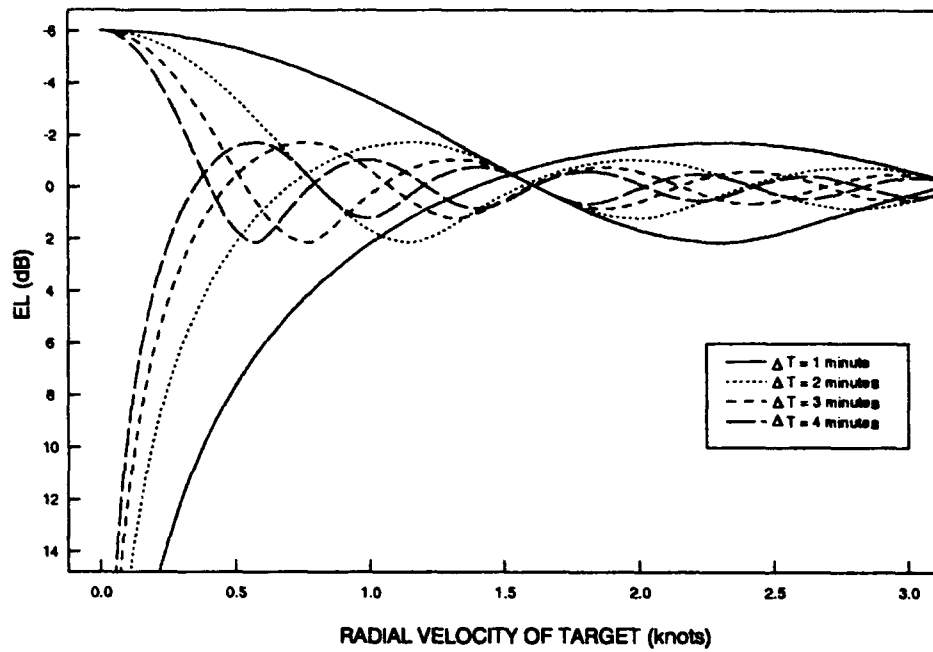


Figure 26. Echo loss envelopes for varying repetition rates.

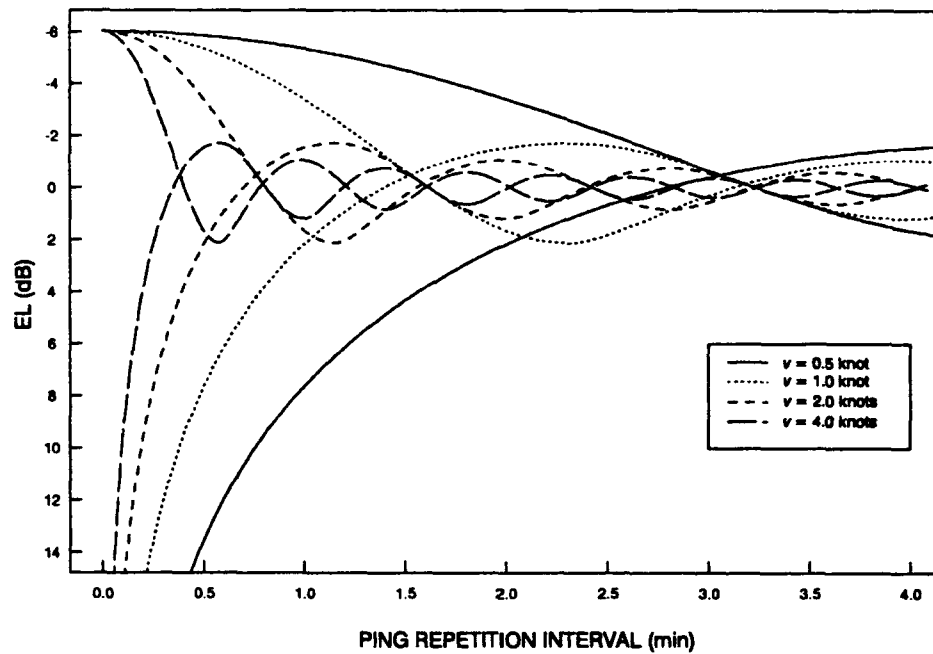


Figure 27. Echo loss envelopes for varying target Dopplers.

GAIN AGAINST REVERBERATION

Now consider the total gain against reverberation (GAR) as a combination of the RPR and all processing losses. This is the total theoretical gain in detectability for a target echo in a distributed reverberation background, processed using interping suppression techniques. Having achieved this gain, the data can then be put through the detector, with a better probability of detection. The gain against reverberation for Case 1 is given by the reverberation power reduction for Case 1, and the target echo loss as

$$GAR_1 = RPR_1 - EL \quad (36)$$

The gain against reverberation for Case 2 is similarly obtained, except that it includes an additional loss term, RL. It is given as

$$GAR_2 = RPR_2 - RL - EL \quad (37)$$

RL is the reference loss due to the input target echo being included in the reference signal, and therefore only applies to Case 2. Because the target echo is in both the input and the reference, it is partially subtracted out in the reverberation processing. So for this case, the output target echo, ϵ_{out} , is equal to the input echo, ϵ_{input} , minus the fraction of the input echo that went into the averaged reference, so that

$$\epsilon_{out} = \epsilon_{input} \left(1 - \frac{1}{N}\right) \quad (38)$$

For detection processing, the signal's power is used. The square of the output echo gives the echo power as

$$P_{\epsilon_{output}} = P_{\epsilon_{input}} \cdot \left(1 - \frac{1}{N}\right)^2 \quad (39)$$

With this result, the loss due to the reference can be determined as the ratio of echo input to output power, in decibels, as

$$RL = 10 \log_{10} \left(\frac{P_{\epsilon_{input}}}{P_{\epsilon_{output}}} \right) = 10 \log_{10} \left[\left(\frac{N-1}{N} \right)^2 \right] \quad (40)$$

Using Eq. 25 and 40, the first two terms of Eq. 37 are simplified as

$$\begin{aligned} RPR_2 - RL &= 10 \log_{10} \left[\frac{N}{(N-1)(1-\Gamma)} \cdot \left(\frac{N-1}{N} \right)^2 \right] \\ &= 10 \log_{10} \left[\frac{N-1}{N} (1-\Gamma) \right] = RPR_1 \end{aligned} \quad (41)$$

This result shows that the overall gain associated with Case 1 and Case 2 is really equivalent, for N total input pings. Thus, while Case 2 suppresses more reverberation than Case 1, it also suffers an additional loss in the target echo. The increased reverberation suppression exactly equals the additional target loss, so they offset one another. Therefore, the final result obtained by using either the method in Case 1 or Case 2 is a gain in detectability given by

$$GAR = RPR_1 - EL \quad (42)$$

VALIDATION WITH DATA

Now actual reverberation data collected by a bistatic receiver off the western coast of the United States are used to validate the interping coherence measurement as a predictor of suppression performance. The target loss effect is not validated with the data, because it does not contain any target echoes. The receiver was fixed on the bottom and located at the base of the rising continental slope. The source was to the east, transmitting a variety of broadband signals in several different frequency bands. The acoustic transmissions, as well as backscattered reverberation from the rising continental slope, were received by the bistatic array. The received signals were processed using an active sonar signal processing software package^[7], in a fashion similar to that described in the Active Sonar Signal Processing section. The received data, the output of coherent reverberation subtraction, measurements of interping coherence, and coherence of reverberation will now be shown.

Figure 28 shows five sequentially received pings, for a single beam looking at the continental shelf. The data have also been matched filtered and smoothed, with the magnitude of the signal power plotted. The received data stream has been segmented from five contiguous blocks of duration $T_{pri} = 90$ seconds and stacked vertically. Stacked in this manner, the pings line up, with the received direct blast located at around 8 seconds. Although the received signals are not calibrated to sound pressure levels, the relative levels show the received signal power fluctuations. Following the direct blast are several areas of significant reverberation power, most noticeably at around 70–85 seconds. This reverberation is backscatter from the rising continental slope. Each of the five received pings shows very similar power characteristics through time. Also notice how the ping repetition interval was chosen to be sufficiently large for the reverberation to die away before the next received ping comes in.

The interping coherence function measurement between ping 1 and ping 2 is shown in figure 29c. From these data it can be seen that the interping coherence is quite high near the direct blast and the shelf reverberation regions. In the other regions, it is lower, because the reverberation power is lower relative to the underlying noise background. Also shown is τ_p , the delay lag of the peak correlation. It can be seen that where the reverberation strongly dominates the noise, the delay values are constant, in this case at -0.02 second. Where the reverberation is not as strong the coherence values drop, and the delay values of the peak are more randomly distributed, as expected. From the measurement of interping coherence, the largest gains against reverberation are expected to be near the direct blast and the shelf regions of the ping.

The interping coherence functions between ping 1 and all the others in the set are shown overlaid in figure 30. The same basic trend is clearly shown by all the plotted coherence functions. In particular, the direct blast is shown to be highly coherent at the same level between all pairs of pings. In addition, the shelf reverberation region, as well as other distinguishable reverberators, shows the same structure. This implies that the interping coherence function is relatively stationary over at least $5T_{pri}$. Hence, for a two-ping subtraction process, equivalent gains against reverberation can be obtained by using a reference ping just before or five pings before the input ping. This stationarity also allows consideration of a multiping subtraction up to at least the five pings shown.

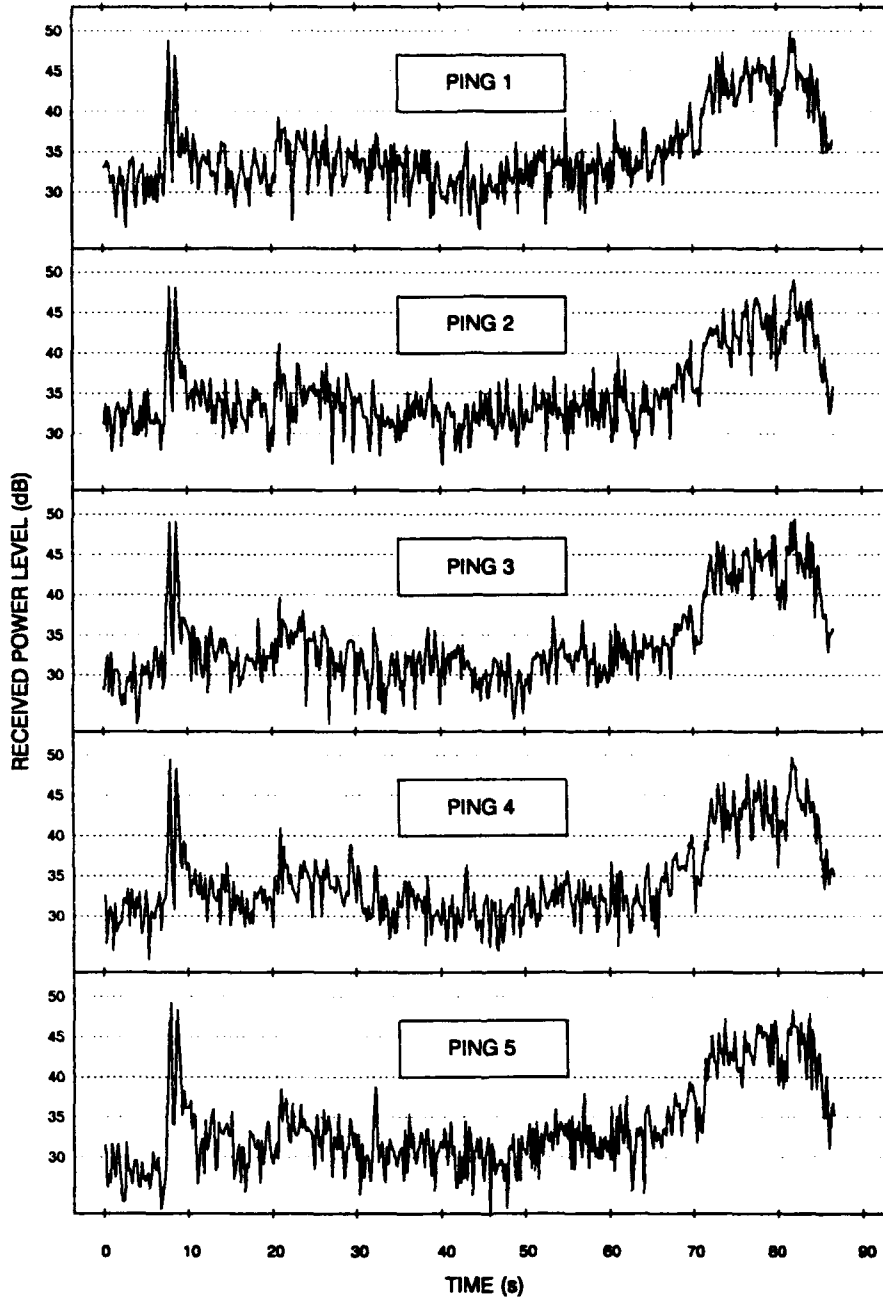
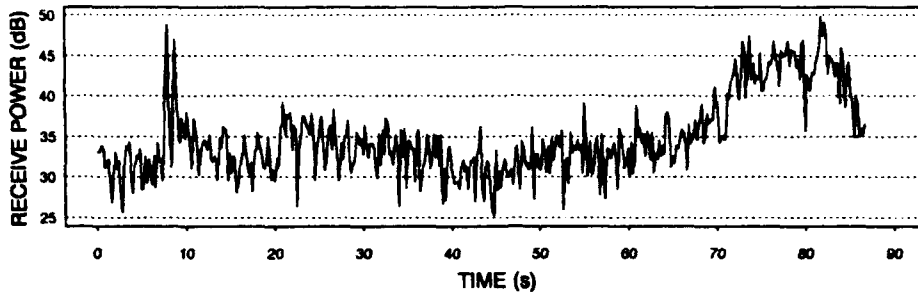
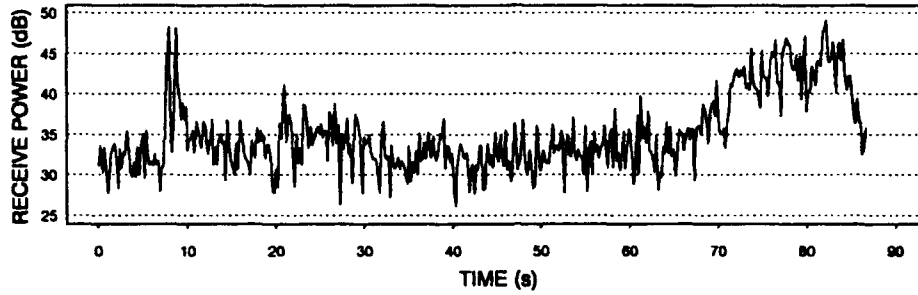


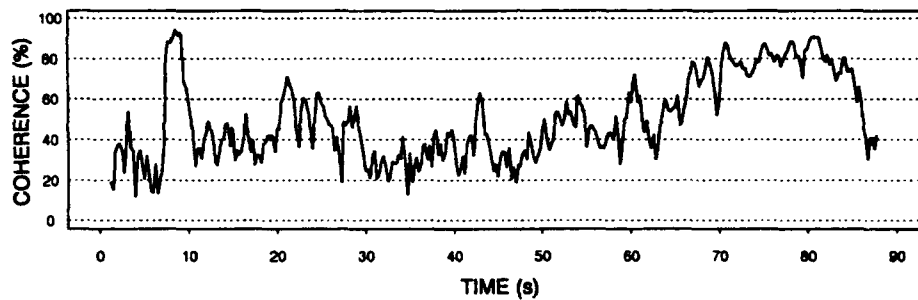
Figure 28. Received ping sequence of reverberation data.



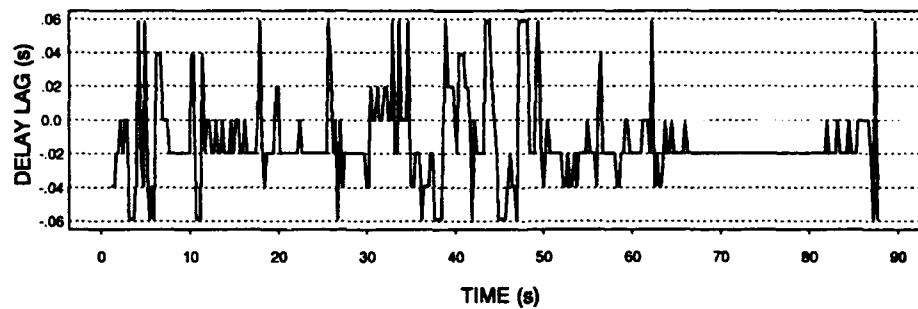
(a) Received ping 1.



(b) Received ping 2.



(c) Interping coherence between (a) and (b).



(d) Delay lag of correlation peak

Figure 29. Interping coherence measurement, ping 1 and ping 2.

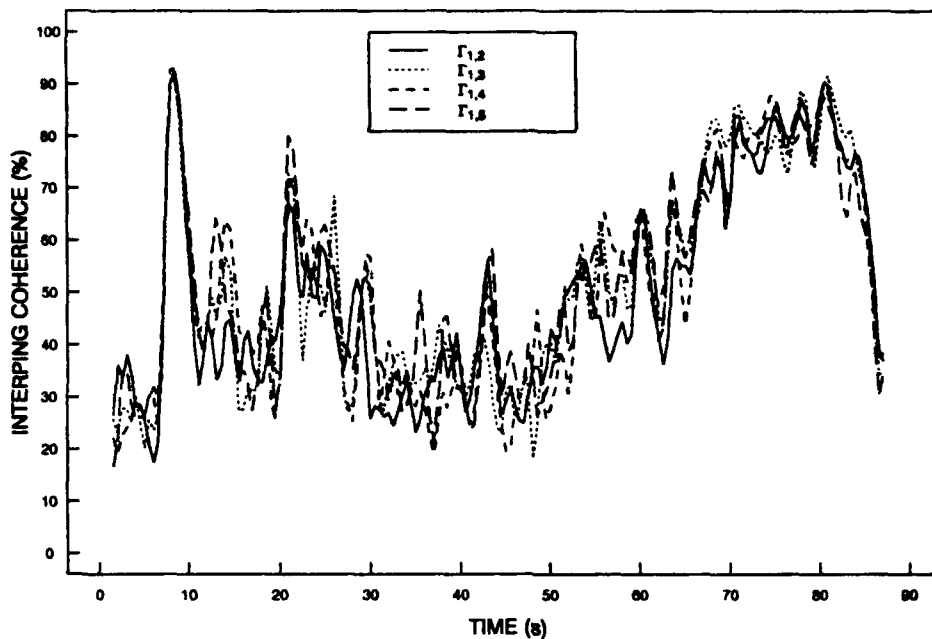


Figure 30. Interping coherence functions.

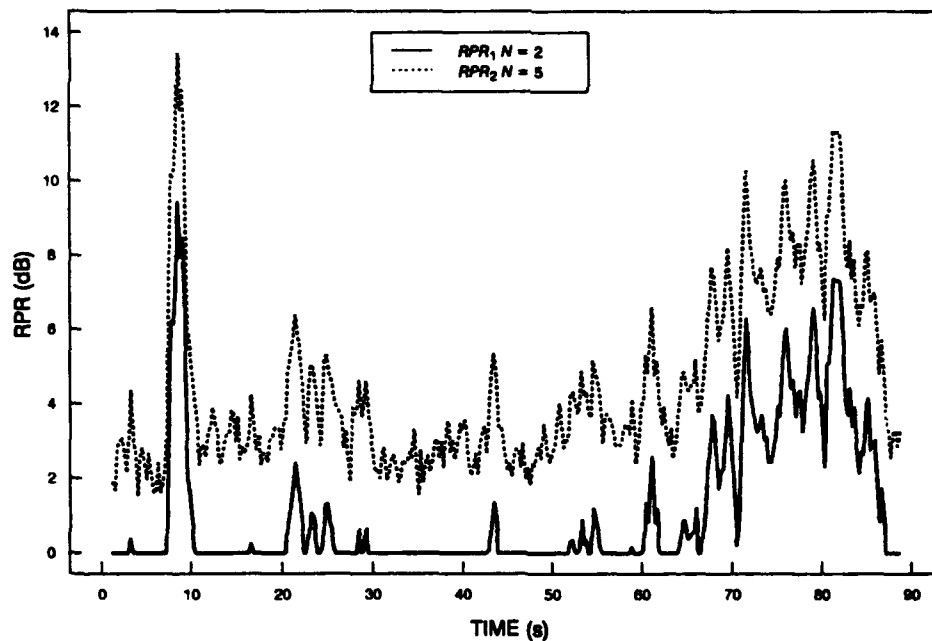


Figure 31. Theoretical reverberation power reduction.

From the interping coherence function measured between pings 1 and 2, the theoretical RPR was calculated by using Eq. 20 and 25. The results are shown in figure 31 for two cases. Case 1 is for a suppression process with two pings, where the input is not a part of the reference. Case 2 is for a process with five pings, with the input included in the reference estimate. The theoretical RPRs near the direct blast and the shelf regions show that significant reductions are possible,

with modest reductions elsewhere. The multiplying process shows larger suppression, as expected. The values of RPR are shown clipped at zero, because in reality the adaptive algorithms are constrained so that they do not yield higher power in the output than the power in the input. These reduction levels predicted by the interping coherence measure are now verified by obtaining the actual reduction levels, using adaptive suppression algorithms.

The data were processed using two different coherent reverberation-suppression algorithms. The first is a two-ping coherent subtraction process with the input ping not included in the reference (Case 1, $N = 2$). The input and reference are pings 1 and 2, respectively, and the RLS adaptive algorithm was used with appropriate choices of parameters. In the second process, the input (ping 1) and the other four pings were input into an SVD algorithm (Case 2, $N = 5$). Figure 32 shows the smoothed power levels of the input ping, along with the suppression outputs for both methods, overlaid. It can be seen that the reverberation power levels are reduced most noticeably in the area of the direct blast and the shelf reverberation. The multiplying method shows more reverberation suppression, as expected.

To quantify the amount of reverberation reduction that these processes have actually achieved, the power levels of the suppression outputs were subtracted from those of the input. This gives the actual RPR obtained by using the algorithms, as shown in figure 33. The actual achieved RPR can then be plotted along with the theoretical RPR, which was obtained using the measured interping coherence. This is shown in figures 34 and 35 for cases 1 and 2, respectively. For both cases, the theoretical RPR closely matches the actual obtained RPR. In this manner, using real reverberation data, the interping coherence function has been validated as an accurate predictor of reverberation reduction.

Finally, the amount of coherence in the reverberation component was estimated by removing from the interping coherence the degradation caused by the noise. Figure 36a shows the received reverberation plus noise level for ping 1. Also shown is the estimated ambient noise level, which is assumed to be constant over the duration of the processing. From this, estimates of the RNNR and Γ_{max} were obtained by using Eq. 26 and 27, respectively. Γ_{max} is shown in figure 36b, along with the measured interping coherence function between pings 1 and 2. Note that there are times when virtually all the possible coherence is being obtained, as well as times when less coherence is achieved. Most noticeably, the direct blast is as coherent as is possible, while the shelf reverberation is not, even though their received power levels are comparable. For the reverberation-limited case, only coherence values above 50% are considered. From these coherence values the coherence of the reverberation, Γ_{reverb} , is obtained by using Eq. 30. This is shown in figure 36c. Notice that the received direct blast is 97% coherent, while the reverberation from the shelf is 80–90% coherent. Also, notice the reverberators at around 53, 60, and 65 seconds. Although they have much smaller power in the received data, they are more coherent than the shelf reverberation. Therefore, this shows that the interping coherence is determined not only by the RNNR, but also by the coherence of the reverberation. In this case, it also shows that it is possible to experience reverberation with varying power levels that have differing coherence values.

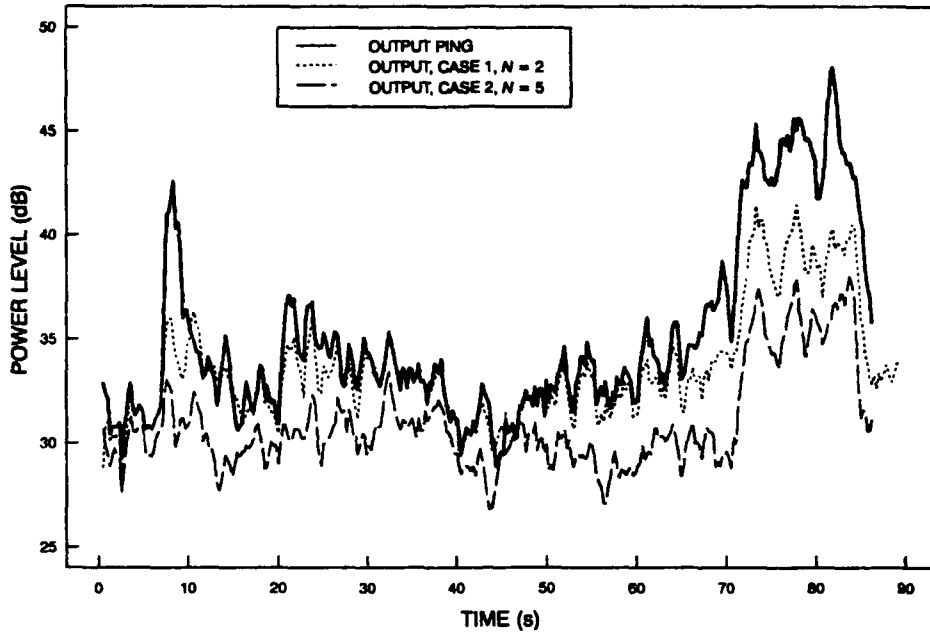


Figure 32. Output of reverberation-suppression processing.

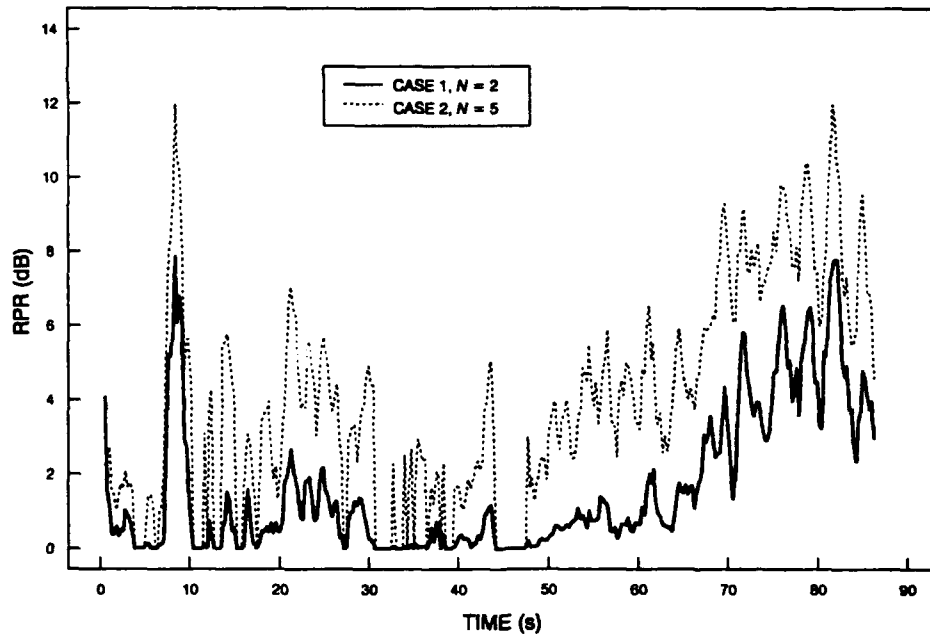


Figure 33. Reverberation power reduction achieved.

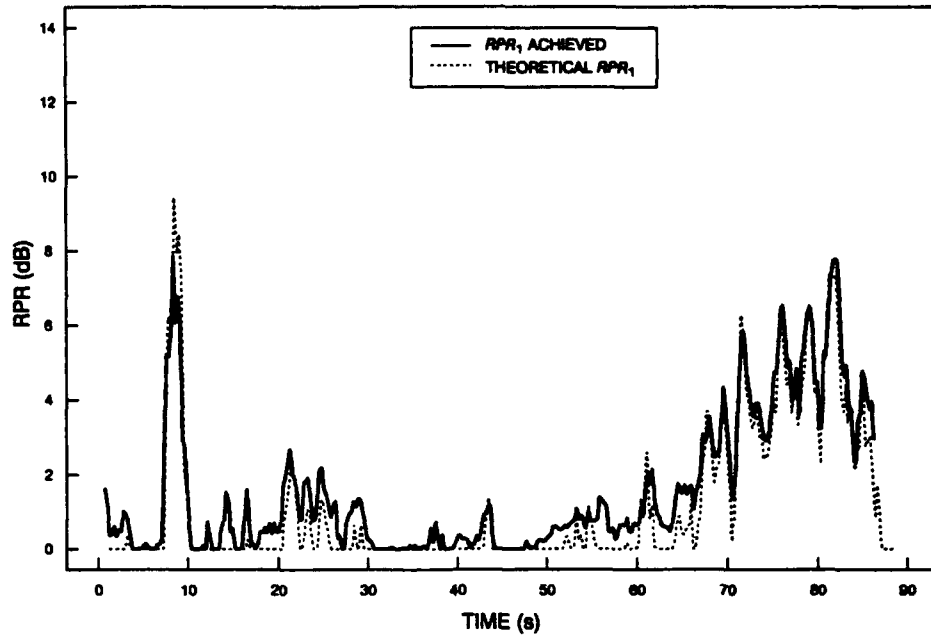


Figure 34. RPR_1 achieved vs. theory ($N = 2$).

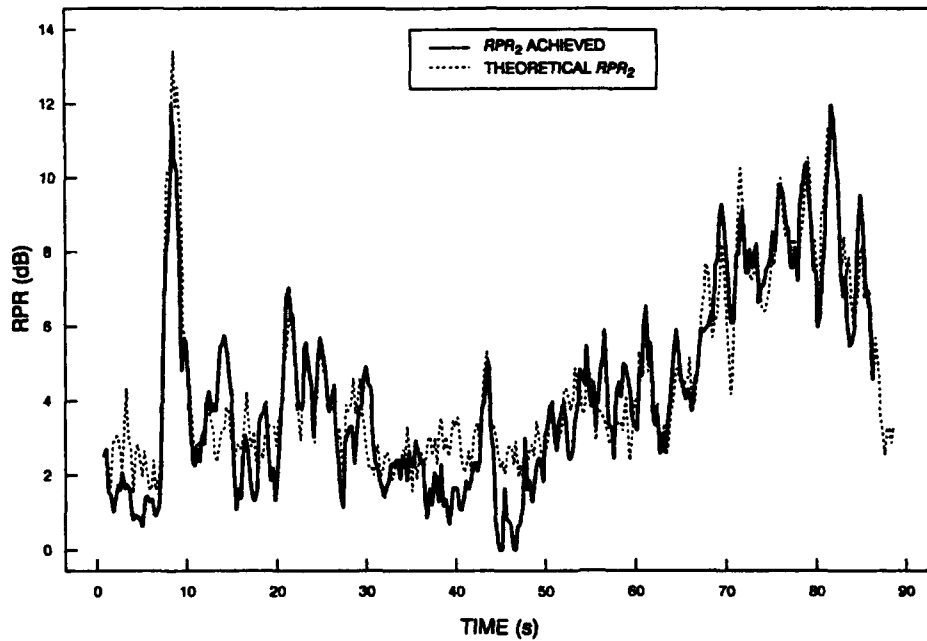
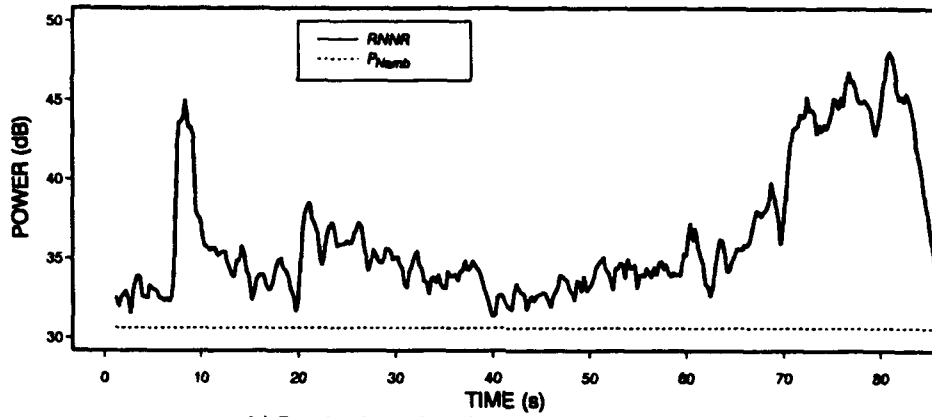
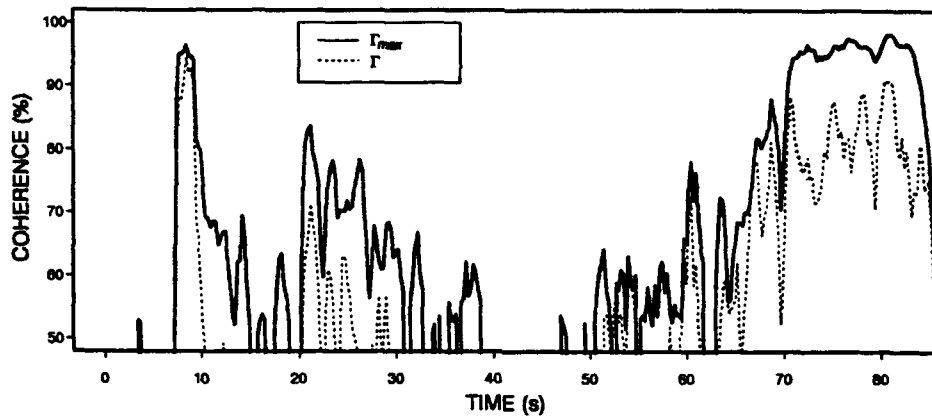


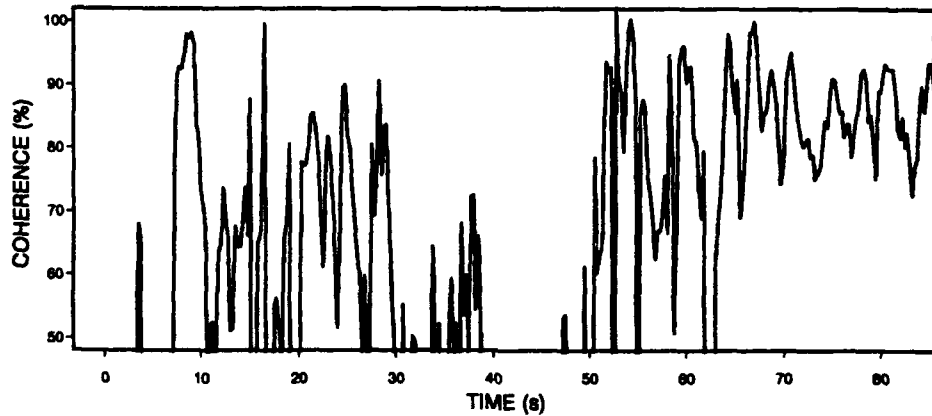
Figure 35. RPR_2 achieved vs. theory ($N = 5$).



(a) Received-reverberation-plus-noise-to-noise level.



(b) Maximum coherence obtainable vs. measured interping coherence.



(c) Coherence of reverberation.

Figure 36. Estimation of coherence of reverberation.

SUMMARY

We have described the approach of applying adaptive interference cancelling techniques to active bistatic sonar data, where reverberation is limiting the detection performance. The performance criteria for both the target echo and the reverberation have been described. The theoretically expected target echo losses were validated with a simulation of synthetically generated target echoes. The interping coherence measure has been shown to be an effective means of predicting the bounds of reverberation suppression. This has been validated by applying the interping coherence measure on actual reverberation data and comparing the predicted RPR with the achieved RPR. This comparison showed very good agreement, indicating that the adaptive algorithms were effectively tuned to obtain the maximum possible performance against reverberation.

REFERENCES

1. Urick, R. J. 1983. *Principals of Underwater Sound*, McGraw-Hill, Chapters 1 and 8, New York, NY.
2. Cox, H. 1988. "Fundamentals of Bistatic Active Sonar," Technical Memorandum No. W1068, BBN System and Technologies Corporation.
3. Widrow, B., J. R. Glover, J. M. McCool, J. Kaunitz, C. S. Williams, R. H. Hearn, J. R. Zeidler, E. Dong, and R. C. Goodlin. 1975. "Adaptive Noise Cancelling: Principals and Applications," *IEEE Proceedings*, Vol. 63, No. 12, pp. 1692-1716 (December).
4. Haykin, S. 1991. *Adaptive Filter Theory*, Prentice-Hall, Englewood Cliffs, NJ.
5. Burdick, W. S. 1991. *Underwater Acoustic System Analysis*, Prentice-Hall, Englewood Cliffs, NJ, p. 209.
6. Bendat, J. S., and A. G. Piersol. 1986. *Random Data: Analysis and Measurement Procedures*. John Wiley & Sons, pp. 114, 127, New York, NY.
7. Moore, S., and X. Zabal. 1991. *DynaLab-RIP: An Interactive Environment for Signal Processing*, Software Package, Science Application International Corporation.

REPORT DOCUMENTATION PAGE

Form Approved
OMB No. 0704-0188

Public reporting burden for this collection of information is estimated to average 1 hour per response, including the time for reviewing instructions, searching existing data sources, gathering and maintaining the data needed, and completing and reviewing the collection of information. Send comments regarding this burden estimate or any other aspect of this collection of information, including suggestions for reducing this burden, to Washington Headquarters Services, Directorate for Information Operations and Reports, 1215 Jefferson Davis Highway, Suite 1204, Arlington, VA 22202-4302, and to the Office of Management and Budget, Paperwork Reduction Project (0704-0188), Washington, DC 20503.

1. AGENCY USE ONLY (Leave blank)		2. REPORT DATE <p style="text-align: center;">December 1993</p>	3. REPORT TYPE AND DATES COVERED <p style="text-align: center;">June 1992—June 1993</p>	
4. TITLE AND SUBTITLE <p style="text-align: center;">PERFORMANCE CRITERIA FOR COHERENT INTERPING REVERBERATION SUPPRESSION</p>			5. FUNDING NUMBERS <p style="text-align: center;">RJ14B24 of ONR CS3A</p>	
6. AUTHOR(S) <p style="text-align: center;">Doug Grimmett and Xavier Zabal</p>				
7. PERFORMING ORGANIZATION NAME(S) AND ADDRESS(ES) <p style="text-align: center;">Naval Command, Control and Ocean Surveillance Center (NCCOSC) RDT&E Division San Diego, CA 92152-5001</p>			8. PERFORMING ORGANIZATION REPORT NUMBER <p style="text-align: center;">TD 2591</p>	
9. SPONSORING/MONITORING AGENCY NAME(S) AND ADDRESS(ES) <p style="text-align: center;">Office of Naval Research 800 North Quincy Street Arlington, VA 22217-5000</p>			10. SPONSORING/MONITORING AGENCY REPORT NUMBER	
11. SUPPLEMENTARY NOTES				
12a. DISTRIBUTION/AVAILABILITY STATEMENT <p style="text-align: center;">Approved for public release; distribution is unlimited.</p>			12b. DISTRIBUTION CODE	
13. ABSTRACT (<i>Maximum 200 words</i>) <p>This report describes the application of adaptive filters to multiping active sonar data for the suppression of reverberation. Interping coherence is described and shown to be a performance predictor for reverberation suppression. Requirements for target echo preservation are also described.</p>				
14. SUBJECT TERMS <p>active sonar reverberation suppression adaptive filters undersea surveillance interping subtraction underwater acoustics ping-to-ping subtraction</p>			15. NUMBER OF PAGES <p style="text-align: center;">50</p>	
17. SECURITY CLASSIFICATION OF REPORT <p style="text-align: center;">UNCLASSIFIED</p>			16. PRICE CODE	
18. SECURITY CLASSIFICATION OF THIS PAGE <p style="text-align: center;">UNCLASSIFIED</p>		19. SECURITY CLASSIFICATION OF ABSTRACT <p style="text-align: center;">UNCLASSIFIED</p>		20. LIMITATION OF ABSTRACT <p style="text-align: center;">SAME AS REPORT</p>

UNCLASSIFIED

21a. NAME OF RESPONSIBLE INDIVIDUAL Doug Grimmett	21b. TELEPHONE (include Area Code) (619) 553-2027	21c. OFFICE SYMBOL Code 732

INITIAL DISTRIBUTION

Code 0012	Patent Counsel	(1)
Code 0274B	Library	(2)
Code 0275	Archive/Stock	(6)
Code 571	M. C. Gillcrist	(1)
Code 572	J. M. Alsup	(1)
Code 572	M. McArthur	(1)
Code 705	M. F. Morrison	(1)
Code 7103	Dr. B. Marsh	(1)
Code 717	A. M. D'Amico	(1)
Code 717	J. W. Douma	(1)
Code 717	D. J. Grimmett	(20)
Code 7205	C. Victory	(1)
Code 726	Dr. C. Persons	(1)
Code 787	Dr. J. C. Lockwood	(1)
Defense Technical Information Center Alexandria, VA 22304-6145 (2)		
Navy Acquisition, Research and Development Information Center (NARDIC) Arlington, VA 22244-5114		
Chief of Naval Operations Washington, DC 20350-2000		
Office of Naval Research Arlington, VA 22217-5660		
Space and Naval Warfare Systems Command 2451 Crystal Drive Arlington, VA 22245-5200 (2)		
Naval Air Warfare Center Warminster, PA 18974-5000		
Naval Oceanographic and Atmospheric Research Laboratory Bay St Louis, MS 39529-5004		
Naval Undersea Warfare Center New London, CT 06320		
Johns Hopkins University Laurel, MD 20723-6099		
Scripps Institution of Oceanography San Diego, CA 92152-6400		
University of Texas at Austin Austin, TX 78713-8029		
Alliant Tech Systems Arlington, VA 22210 (2)		
Alliant Tech Systems San Diego, CA 92111 (2)		
American Telephone and Telegraph, Co. Bell Laboratories Whippany, NJ 07981		
Science Applications International Corporation McLean, VA 22102		